MATERIALS AND DESIGN SELECTION OF NFC FILAMENT FOR THE SHARK FIN ANTENNA USING HYBRID METHOD

UNDERGRADUATE THESIS

Submitted to the International Undergraduate Program in Mechanical Engineering in Partial Fulfillment of Requirement for the Degree of Sarjana Teknik at the Faculty of Industrial Technology

Written by:

Name : Muhammad Mizan Abhiyasa

Student Number : 21525063

NIRM :

UNDERGRADUATE PROGRAM IN MECHANICAL ENGINEERING
FACULTY OF INDUSTRIAL TECHNOLOGY
UNIVERSITAS ISLAM INDONESIA
YOGYAKARTA
2025

SUPERVISOR APPROVAL SHEET

MATERIALS AND DESIGN SELECTION OF NFC FILAMENT FOR THE SHARK FIN ANTENNA USING HYBRID METHOD

UNDERGRADUATE THESIS

Written by:

Name : Muhammad Mizan Abhiyasa

Student Number : 21525063

NIRM :

Yogyakarta, July 21, 2025

Supervisor I,

Ir. Arif Budi Wicaksono S.T., M.Eng., IPP

Supervisor II,

Ts. Dr. Mohd Adrinata Bin Shaharuzaman

EXAMINERS APPROVAL PAGE

MATERIALS AND DESIGN SELECTION OF NFC FILAMENT FOR THE SHARK FIN ANTENNA USING HYBRID METHOD

UNDERGRADUATE THESIS

Written by:

Name : Muhammad Mizan Abhiyasa

Student Number : 21525063

NIRM :

Examiners

Dr. Ts. Mohd Hanif bin Harun ______________

Examiner I Date :

Ir. Ts. Dr. Fauzi bin Ahmad ______________

Examiner II Date :

Acknowledged by

Head of Mechanical Engineering Department

Dr. Ir. Muhammad Khafidh, S.T.,M.T., IPP

AUTHENTICITY STATEMENT

In the name of Allah SWT, I declare this work is the result of my own, except for the those which I have explained the source. If, in the future, it turns out that my declaration is proven to be untrue and violates the legal regulations in the paper and intellectual property rights, in that case, I am willing to get diploma that I have received to be withdrawn by the Universitas Islam Indonesia.

Yogyakarta, July 21, 2025

Muhammad Mizan Abhiyasa

2125063

DEDICATION PAGE

First and foremost, I wish to express my gratitude to Allah for his blessing in the completion of this work, despite the challenges encountered during this study. I would want to express my gratitude to my beloved parents, who consistently support me from a distance and wish me well. I would like to express my gratitude to my supervisors, Ts Dr. Mohd Adrinata bin Shaharuzaman and Ir. Arif Budi Wicaksono, for their guidance and patience in assisting me.

MOTTO

"Allah does not require of any soul more than what it can afford."
(QS. Al-Baqarah: 286)

"You do not know what you are capable of until you try — even if it costs you your life." – Sultan Mehmed II

PREFACE

Assalamu'alaikum Warahmatullaahi Wabaraakatuh

The author expresses gratitude for the presence of Allah SWT, the Lord of all worlds, who has bestowed His love and guidance. Blessings and peace are continuously sent to Prophet Muhammad SAW, a role model who has led humanity to an era of greatness. With the permission and will of Allah, the author has completed the undergraduate thesis titled "Materials and Design Selection of NFC filament for the Shark Fin Antenna Using Hybrid Method" Additionally, the author would like to express gratitude to:

1. To my beloved parents who always support the author, giving motivation in every step of this academic journey, also, to my siblings who always support the author.
2. Ir. Arif Budi Wicaksono as the supervisor from Universitas Islam Indonesia, for his valuable guidance throughout the study.
3. Ts. Dr. Adrinata bin Shaharuzaman as the supervisor from University Teknikal Malaysia Melaka, who helped the author to overcome every challenge during the study.
4. To my senior, Edo Bagus Rachmat Dwiputra, for his generous assistance and guidance.

ABSTRACT

This study demonstrates the application of natural fiber composite (NFC) filaments in the manufacture of shark fin antennas via 3D printing technology. The research commences with three conceptual designs developed with SolidWorks, a computer-aided design (CAD) software. The designs are being evaluated for their aerodynamic qualities using Solidworks Flow Simulation tools. The Technique for Order Preference by Similarity to Ideal Solution (TOPSIS) is employed to evaluate a dataset. The rank with the highest value of C_i is selected as number one. Design 3 is chosen because to its superior C_i value of 0.995, accompanied by a drag force of 0.457 N, a coefficient of drag of 0.457 N, and a surface pressure of 101821.69 Pa. The NFC filaments PLA/Wood are printed using the fused deposition method (FDM) in compliance with ASTM D638 for tensile test and ASTM D790 for flexural test. The characteristics fluctuate at infill densities of 50%, 75%, and 100%. Fifteen specimens are being printed, with five specimens allocated for each parameter. The experimental results were recorded and tabulated with data from a prior study involving PLA/Coconut and PLA/Bamboo. The TOPSIS approach is employed to identify the optimal material for the shark fin antenna. PLA/Wood was identified as the optimal material, exhibiting the greatest C_i value of 0.6025, a tensile strength of 37.46 MPa, a tensile Young's modulus of 1663 MPa, a flexural stress of 65.187 MPa, a modulus of elasticity of 2694 MPa, and a cost of RM 72.00. Finally, the shark fin antenna is produced by 3D printing based on specific design and material specifications. The study indicates that the mechanical properties of natural fiber composites can be determined by mechanical testing in accordance with ASTM standards. Conversely, the TOPSIS technique is applicable when selecting from several alternatives based on various criteria.

Keywords: Natural Fiber Composite (NFC), 3D Printing, Shark Fin Antenna, TOPSIS Method, Mechanical Properties.

TABLE OF CONTENTS

LIST OF TABLES

LIST OF FIGURES

LIST OF SYMBOLS

3D	=	3 Dimension
mm	=	Millimeter
N	=	Newton
mm/min	=	Millimeter Per Minute
Pa	=	Pascal
MPa	=	Mega Pascal
m/s	=	Meter Per Second
m^2	=	Meter Square
RM	=	Ringgit Malaysia
%	=	Percent
°C	=	Degree Celsius

CHAPTER 1
INTRODUCTION

1.1 Background

The automotive industry has increasingly embraced lightweight and sustainable materials to meet higher environmental regulations, improve fuel efficiency, and enhance overall performance. Among these materials, Natural Fiber Composites (NFCs) have gained considerable attention automotive applications due to their renewable nature, biodegradability, low density, and excellent specific mechanical properties. NFCs are composites where natural fibers such as jute, flax, kenaf, or hemp are used as reinforcements in polymer matrices. These composites present a sustainable alternative to conventional synthetic fiber composites like glass or carbon fiber.

Recent advancements in additive manufacturing (3D printing) have further expanded the potential of NFCs in automotive applications. The development of NFC filaments suitable for 3D printing enables the fabrication of complex geometries and customized components with reduced material waste. Studies have demonstrated the feasibility of 3D printing NFCs, highlighting their mechanical strength, thermal stability, and environmental advantages (Khilji et al.,2023)

A review by Bi and Huang (2022) supports the viability of natural fiber–based filaments in additive manufacturing, pointing to their compatibility with extrusion-based 3D printing methods and favorable mechanical behavior. Moreover, NFCs exhibit good interfacial bonding with biopolymers such as PLA, which are commonly used in sustainable manufacturing processes.

Shark fin antennas are multipurpose parts that are frequently found on the roofs of vehicles and house cellular networks, GPS, and radio systems, among other communication systems. NFCs have historically been produced with materials like ABS plastic, however there is increasing interest in investigating them for this use. Incorporating NFCs into shark fin antenna housings offers advantages for the environment as well as chances for enhanced performance and visual personalization (Sahib Dua et al., 2023)

In the context of automotive components, the adoption of NFCs for shark fin antennas necessitates a comprehensive approach to material and design selection. Factors such as mechanical performance, weather resistance, electromagnetic compatibility, and manufacturability must be considered. Employing a hybrid method that combines multiple criteria decision-making techniques can facilitate the optimal selection of NFC materials and design parameters (Elseify et al., 2021).

Furthermore, the life cycle assessment (LCA) of NFCs indicates a lower environmental impact compared to conventional materials. A study by Sahib Dua et al. (2023) investigates the potential of cellulosic fiber-based polymeric composites for automotive applications, highlighting their contribution to cleaner production processes and reduced carbon footprint.

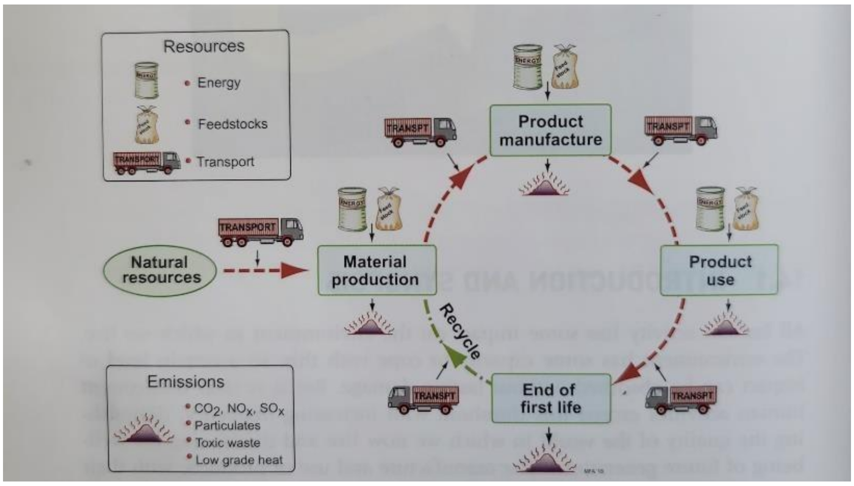

Figure 1-1 The Material life-cycle
(Ashby, 2017)

The exploration of NFCs for shark fin antenna applications presents a promising avenue for sustainable automotive design. The combination of natural fiber materials, advanced manufacturing techniques like 3D printing, and comprehensive material selection methodologies can lead to the development of environmentally friendly, high-performance automotive components.

1.2 Problem Formulation

Based on the background of the research that has been explained, we can formulate some research questions:

1. How to determine the optimal design of a shark fin antenna using simulation and multi-criteria decision-making methods?
2. How is the mechanical performance of different NFC filaments when tested according to ASTM standards?
3. How to identify the most suitable NFC filament material for shark fin antennas using the hybrid method?

1.3 Research limitations

The following are the limitations of the research:

1. The data used in this thesis research is based on experiment at Universiti Teknikal Malaysia Melaka (UTeM).
2. The velocity applied for Shark Fin Antenna is 90.15 km/h
3. The infill percentage is vary, from 50%, 75% to 100%.
4. The design and material selection used in the research is The Technique for Order of Preference by Similarity to Ideal Solution (TOPSIS)
5. The software to support the research is Solidworks with Bambu Studio for slicing process

1.4 Research Objectives

The objectives of this project are as follows:

1. To analyze the mechanical properties of the NFC filament
2. To evaluate the conceptual design of the Shark fin antenna using a hybrid method (CAD and MCDM)
3. To fabricate the Shark fin antenna using FDM method

1.5 Benefits of Research

Benefits of this research are:

1. This research is beneficial for the manufacturing industry as it provides a systematic method for selecting the optimal material and design for shark fin antennas, enhancing both performance and cost efficiency.
2. The findings can serve as a reference for other researchers or companies developing 3D-printed products using natural fiber composite filaments, encouraging sustainable material usage.
3. The benefit for the student is that this research develops skills in CAD design, simulation analysis, decision-making methods such as TOPSIS, and compliance with ASTM testing standards.
4. This research can contribute to the academic field by providing comparative data on the mechanical properties of different NFC filaments, which can be used for future studies in material science and additive manufacturing.

1.6 Systematic Research

The research is structured into several chapters, and each chapter will be described as follows:

CHAPTER I INTRODUCTION

This chapter discusses the background of the research conducted, problem formulation based on the background, problem limitations, research objectives, research benefits, and systematic writing of the research conducted.

CHAPTER II LITERATURE REVIEW

This chapter covers the theoretical foundation of research development derived from deductive analysis and elucidates inductive studies by contrasting summaries of prior research.

CHAPTER III RESULT METHODOLOGY

This chapter discusses the subjects and objects of research, types of data used, research instruments, data collection methods, data processing methods, data analysis methods, and flowcharts of the research conducted.

CHAPTER IV RESULTS AND DISCUSSION

This chapter discusses the data collection process, data obtained during the research, and data processing that has been obtained using the methods used in the research.

CHAPTER V CLOSING

This chapter discusses the conclusions of all the results obtained that answer the research objectives and suggestions for the research that has been carried out for further research.

CHAPTER 2
LITERATURE REVIEW

2.1 Literature Review

This chapter talks about the shark fin antenna in general and how it is used in cars, especially to improve the aerodynamics of the car and the reception of signals. This chapter also talks about the basics of antenna design and looks at how roof-mounted attachments like the shark fin antenna affect the way the car moves through the air. The usage of 3D printing technology is also talked about, with a focus on Fused Deposition Modelling (FDM) as a way to make prototype antennas. This chapter also talks about composite materials and how they might be used in antenna constructions, such as the best filaments for 3D printing. The morphological approach to concept design is also provided, as well as the way for applying Flow simulation tools, to simulate airflow and signal performance. The Technique for Order of Preference by Similarity to Ideal Solution (TOPSIS) method will be used for the process of selection and evaluation. Finally, the mechanical tests used to check how well materials work are spoken about, with a focus on tensile and flexural tests that are important for the strength and endurance of antennas.

2.2 Theoretical Basis

2.2.1 Natural Fiber Composites (NFC) in Engineering Applications

Natural Fiber Composites (NFCs) have emerged as a promising category of materials due to their potential for sustainability, lightweight properties, and wide range of applications in engineering. These composites, typically composed of plant-based fibers and a polymer matrix, offer an eco-friendly alternative to synthetic fiber-reinforced composites. Increasing environmental concerns and a push for greener technologies have led to growing interest in NFCs for industries such as automotive, aerospace, construction, and packaging (Zulkifli et al., 2023).

Natural fibers, sourced from renewable plant materials such as hemp, jute, kenaf, sisal, and flax, are primarily composed of cellulose, hemicellulose, lignin, and pectin. These fibers can be categorized into bast, leaf, seed, and fruit fibers depending on their origin. They offer low density, good specific strength, and biodegradability, which make them attractive for various structural and semi-structural applications (Jumaidin et al., 2021).

A critical factor influencing the performance of NFCs is the nature of the fiber, including its mechanical properties, surface chemistry, and compatibility with the matrix. Effective fiber treatment processes such as alkaline treatment and silane coupling agents are often employed to enhance fiber-matrix adhesion, thereby improving the composite's mechanical strength and durability (Kulkarni et al., 2021).

2.2.2 Advantages and Limitations of NFC

The advantages of NFCs are substantial. They include low weight, reduced cost, biodegradability, good acoustic and thermal insulation properties, and a lower carbon footprint compared to conventional composites (Shadrach et al., 2021). NFCs also offer ease of processing using existing manufacturing techniques, making them suitable for mass production. In biomedical applications, their biocompatibility and renewability further enhance their value (Singh et al., 2023).

Despite these benefits, NFCs face several limitations. One major challenge is their high moisture absorption, which can lead to dimensional instability and reduced mechanical performance. They also generally have lower impact resistance and thermal stability compared to synthetic fiber composites.

Additionally, inconsistencies in fiber quality due to agricultural variability and the need for surface treatment increase production complexity (Azman et al., 2021).

Efforts to overcome these limitations include hybridization with synthetic fibers, the development of advanced bio-resins, and ongoing research into fiber modification techniques. These advancements are essential to expanding the applicability of NFCs in more demanding industrial sectors.

2.2.3 Polylactic Acid (PLA)

Polylactic Acid (PLA) is a biodegradable, bio-based thermoplastic polyester that has gained significant attention for its application in 3D printing and biomedical engineering due to its favorable mechanical properties, ease of processing, and environmental friendliness (Khouri et al., 2024). PLA exhibits a high tensile modulus and flexural strength compared to common polymers like polypropylene and polyvinyl chloride, and its mechanical properties can be further enhanced through processes such as annealing or by incorporating reinforcing agents (Satsum et al., 2022). The material's performance in additive manufacturing is highly sensitive to process parameters such as layer height, infill density, print speed, and extrusion temperature, with optimization studies demonstrating that careful adjustment of these factors can significantly improve tensile strength and overall print quality (Jatti et al., 2024). PLA's structure can be tailored through stereochemistry and molecular weight adjustments, allowing for the production of both amorphous and semi-crystalline forms, which affects its thermal and mechanical behavior. Its transparency, stability at low temperatures, and good barrier properties make PLA suitable for a range of applications, including packaging, disposable products, and medical devices, while its biodegradability positions it as a sustainable alternative to petroleum-based plastics (Ranakoti et al., 2022).

2.2.4 PLA /wood

The mechanical performance of PLA/Wood composites has been a primary focus in the literature. Studies show that the addition of wood fibers can increase stiffness and dimensional stability, but often at the expense of tensile strength and ductility compared to pure PLA (Bhayana et al., 2023). For example, PolyWood™ exhibits a tensile strength of 20.31 MPa and a flexural strength of 31.36 MPa, which are lower than those of pure PLA but comparable to some wood composites (Fauzi et al., 2024). The presence of wood content generally reduces density, making the material lighter, but can also introduce brittleness and lower mechanical strength, especially at higher wood loadings

PLA/Wood filament typically consists of a PLA base material mixed with varying amounts of wood particles. The wood content varies by manufacturer, ranging from approximately 30% in most brands to as high as 40-45% in premium options such as Nanovia's PLA/Wood. These wood particles are often derived from sustainable sources, with some brands like Nanovia using pine wood powder from up-cycled fallen trees in the French Landes region. Table 2.1 shows the mechanical properties of PLA-based composites.

Table 2-1 Mechanical Properties of PLA-Based Composites
(Ayyub, 2022)

Material	**TS (MPa)**	**YM (GPa)**	**FS (MPa)**	**FM (GPa)**	**VMS (N/m^2)**	**DP (mm)**
PLA/ Bamboo	32.83	4.88	41.04	1.07	2.114	1.333
PLA/ Coconut	30.70	5.20	39.36	1.46	2.114	1.250
PLA/ Wood	36.62	5.34	37.18	1.18	2.114	1.218
PLA/ Metal	53.65	6.26	70.23	2.71	2.114	1.039

TS: Tensile Strength, YM: Young Modulus, FS: Flexural Strength, FM: Flexural Modulus, VMS: Von Mises stress, DP: Displacement

2.2.5 Material and Design Selection

Hybrid Multi-Criteria Decision-Making (MCDM) methods integrate complementary techniques to address complex material and design selection problems. These methods are particularly effective in scenarios involving conflicting criteria, interdependencies, and uncertainty. Shown in table 2.2

Table 2-2 Comparison Methods in MCDM

Aspect	TOPSIS	VIKOR	Fuzzy Methods
Full Name	Technique for Order of Preference by Similarity to Ideal Solution (Pavić & Novoselac, 2013)	VlseKriterijumska Optimizacija I Kompromisno Resenje (Multicriteria Optimization and Compromise Solution)	Fuzzy Logic-based Multi-Criteria Decision Making
Core Principle	Ranks alternatives by measuring geometric distance from ideal and anti-ideal solutions, selecting the alternative closest to positive ideal and farthest from negative ideal	Identifies compromise solutions closest to ideal solution while maximizing group utility and minimizing individual regret (Xu et al., 2024)	Handles uncertainty and imprecision using membership functions to represent linguistic variables and vague information

Aspect	TOPSIS	VIKOR	Fuzzy Methods
	(Pavić & Novoselac, 2013)		(Sahoo et al., 2024)
Decision Strategy	Compensatory approach allowing trade-offs between criteria - poor performance in one criterion can be offset by good performance in another (Pavić & Novoselac, 2013)	Non-compensatory compromise approach focusing on balanced solutions that satisfy majority while minimizing opposition (Xu et al., 2024)	Flexible approach accommodating linguistic assessments and uncertain information through fuzzy reasoning (Sahoo et al., 2024)
Computational Complexity	Relatively simple with straightforward calculations - construct decision matrix, normalize, weight, calculate distances, and rank	Moderate complexity requiring calculation of utility, regret, and compromise indices with additional stability conditions (Taherdoost & Madanchian, 2023)	Variable complexity depending on fuzzy operations used, generally more complex due to membership function evaluations (Güçlü, 2024)

Table 2-2 simplifies Comparison Methods in MCDM (Continued)

Advantages	Simple and intuitive methodology; efficient for large datasets; flexible adaptation to various problems; clear geometric interpretation	Provides compromise solutions balancing group utility and individual regret; includes stability conditions for robust decisions; handles conflicting criteria effectively (Taherdoost & Madanchian, 2023)	Handles uncertainty and imprecision naturally; accommodates linguistic variables; provides flexible framework for qualitative assessments (Al Mohamed et al., 2023)
Disadvantages	Sensitive to weight assignments; compensation effect may not always be desirable; requires precise numerical inputs	Sensitive to weight coefficients; requires additional parameters (strategic weight ν); may not identify unique solutions (Taherdoost & Madanchian, 2023)	Computational complexity increases with fuzzy operations; requires expertise in membership function design; subjective in fuzzy rule formulation (Güçlü, 2024)

Table 2-2 simplifies Comparison Methods in MCDM (Continued)

Ranking Behavior	More compensatory behavior - allows significant trade-offs between criteria (Sanchez-Lozano et al., 2022)	Less compensatory - influenced more heavily by most important criteria, seeks balanced solutions (Sanchez-Lozano et al., 2022)	Adaptable behavior depending on fuzzy rule design and membership functions used (Sahoo et al., 2024)
Application Suitability	Best for scenarios requiring clear ideal solutions with measurable criteria; effective in supplier selection, material selection (Vassoney et al., 2021)	Optimal for conflict resolution scenarios requiring compromise solutions; suitable for group decision making with diverse stakeholder interests	Ideal for problems with uncertain, imprecise, or linguistic information; excellent for qualitative assessments (Al Mohamed et al., 2023)
Validation Requirements	Requires sensitivity analysis for weight variations; correlation analysis for ranking consistency (Servaitė, Užupytė,	Needs verification of acceptable advantage and decision stability conditions; sensitivity analysis for parameter variations (Xu et al., 2024)	Requires validation through scenario testing and membership function sensitivity analysis

	& Krilavičiusa, 2020)		(Sanchez-Lozano et al., 2022)
Hybrid Applications	Commonly integrated with AHP for weighting, fuzzy logic for uncertainty handling (Sanchez-Lozano et al., 2022)	Often combined with DEMATEL, ANP, or fuzzy approaches for enhanced decision support (Sanchez-Lozano et al., 2022)	Frequently hybridized with TOPSIS, VIKOR, or AHP to create robust fuzzy MCDM frameworks (Erdebilli et al., 2023)

2.2.6 Finite Element Method in Engineering

Finite Element Method (FEM) represents one of the most significant developments in computational methods for engineering analysis. According to Erhunmwun and Ikponmwosa, FEM was first used in 1956 for aircraft structural analysis, and within a decade, its potential for solving various types of engineering and applied science problems was widely recognized. The method involves discretizing complex problems and analyzing them part by part, with its power lying in its ability to provide accurate solutions regardless of problem geometry, given proper mesh refinement (Erhunmwun & Ikponmwosa, 2017).

The finite element technique has become well-established as one of the best methods for analyzing the efficiency of a wide variety of problems (Erhunmwun & Ikponmwosa, 2017). It operates by breaking complex systems into smaller, simpler pieces or elements, then applying differential equations to each element individually, effectively dividing and conquering engineering problems. This numerical technique finds approximate solutions to boundary value problems for partial differential equations, and is also referred to as finite element analysis (FEA) (Saurabh & Yadav, 2016).

Recent advances in FEA include the development of mesh-free methods for solving complex problems. One such approach is the mesh-free least-squares-based finite difference (LSFD) method used for solving large amplitude free vibration problems of arbitrarily shaped thin plates. This method is particularly useful for solving problems with complex domain geometries due to its mesh free and local approximation characteristics (Saurabh & Yadav, 2016). A key advantage of FEA is its ability to assess complex geometries that would otherwise be challenging or impossible to evaluate. It can analyze any shape geometry, from simple blocks to complex structures like the human heart, at any size scale from nanoscale to large passenger jets, and with any type of physics from heat transfer to fluid dynamics and structural mechanics.

2.2.7 Finite Element Analysis in Tensile Testing

Researchers have examined how specimen shapes influence stress distribution in FDM printed ASTM D638 dog-bone specimens. Rectangular geometries based on composite standard ASTM D3039 reduced stress concentrations compared to curved-neck dog-bones, yielding higher tensile strength and modulus in FEA simulations, particularly for edge-built parts (Faidallah et al., 2023).

Additive manufacturing (AM) studies used FEA to analyze tensile behavior of PLA specimens with embedded internal features. Simulations accurately predicted ultimate tensile strength (UTS) and strain at UTS by incorporating defect geometry into the mesh, guiding nondestructive monitoring approaches (AbouelNour et al., 2024).

Finite element models of fly-ash/HDPE and fly-ash/PP hybrid composites under ASTM D638 loading conditions revealed that increasing filler content altered stress–strain response. FEA predicted reductions in yield strength and tensile modulus, matching experimental trends and highlighting the importance of material homogenization techniques in RVE selection (Zulkifli et al., 2020).

Studies on 3D-printed PLA specimens evaluated the influence of infill patterns (rectangular, hexagonal, diamond) via FEA and experiment. Hexagonal patterns yielded the highest UTS and toughness in simulations by optimizing load paths within the gauge section, corroborating physical tests (Harpool et al., 2021).

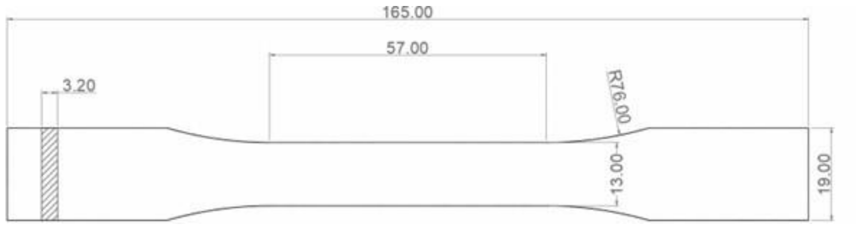

Figure 2-1 Geometry of specimen according to Type I: ASTM D638 (García-Domínguez et al., 2019)

2.2.8 Finite Element Analysis in Flexural Testing

FDM-printed PET-G specimens were subjected to three-point bending FEA under ASTM D790. Response surface models integrated layer height, infill density, deposition angle, and print temperature. FEA revealed that solid infill at 0° deposition angle maximized flexural strength, guiding optimal print settings for PET-G components (Fountas et al., 2021).

Three-point bending FEA of polymer matrix composites reinforced with continuous fibers or sandwich cores predicted flexural moduli and failure loads within 5% of experimental values. Models using orthotropic properties for static loading accurately captured debonding and delamination in glass-fiber sandwich panels, validated against ABAQUS simulations and mechanical tests (Alshahrani & Ahmed, 2022).

Hybrid composites combining S2-glass fibers with graphene oxide nanofillers were evaluated by FEA to assess flexural load capacity. Simulations showed synergistic stress redistribution at fiber–matrix interfaces that increased flexural strength by 20%, aligning with test results for aerospace-grade materials

FEA-based modal and strain energy analyses under bending loads enabled non-destructive damage detection in metallic dampers and concrete beams. Changes in modal frequencies and strain energy distributions corresponded to stiffness loss, demonstrating FEA’s utility for structural assessment beyond material characterization.

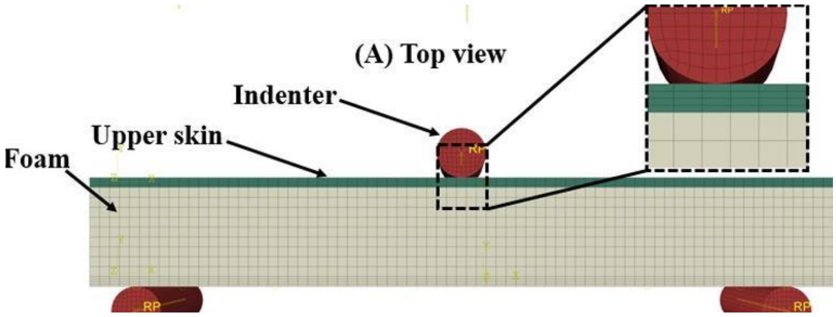

Figure 2-2 Three-point bending test system
(Alshahrani & Ahmed, 2022).

2.2.9 Additive Manufacturing Technology

Additive manufacturing (AM), colloquially termed 3D printing, encompasses a suite of technologies that fabricate objects layer-by-layer from digital models, revolutionizing traditional subtractive and formative manufacturing paradigms. The American Society for Testing and Materials (ASTM) categorizes AM into seven distinct processes: material jetting (MJ), binder jetting (BJ), vat photopolymerization (VP), powder bed fusion (PBF), material extrusion (ME), directed energy deposition (DED), and sheet lamination (SL) (Wu et al., 2022). Each technology employs unique mechanisms to deposit and solidify materials, ranging from photopolymer curing in VP systems like stereolithography (SLA) to laser sintering of powders in PBF methods such as selective laser sintering (SLS) (Koltsaki & Mavri, 2024).

Material extrusion, particularly fused deposition modeling (FDM), has gained prominence due to its affordability and versatility in processing thermoplastics (Vyavahare & Teraiya, 2020). Conversely, PBF and DED are favored for high-strength metal parts in aerospace and biomedical applications, albeit with higher costs and post-processing requirements (Wu et al., 2022). Vat photopolymerization, including digital light processing (DLP), excels in producing high-resolution prototypes but is limited by material brittleness (Rasiya et al., 2021). The evolution of AM technologies has been driven by advancements in materials, precision, and multi-material capabilities, enabling applications in rapid prototyping, customized medical implants, and complex aerospace components (Zhai et al., 2022).

2.2.10 Fused Deposition of Modeling (FDM)

Fused deposition modeling (FDM), a subset of material extrusion, operates by heating thermoplastic filaments to a semi-molten state and depositing them through a nozzle onto a build platform (Vyavahare & Teraiya, 2020). The process begins with a 3D model sliced into layers, with G-code dictating parameters such as nozzle temperature, layer height, and printing speed. Common materials include polylactic acid (PLA), acrylonitrile butadiene styrene (ABS), and polyethylene terephthalate glycol (PETG), chosen for their thermal stability and mechanical properties (Medibew & Tesfaye, 2022).

Critical challenges in FDM include anisotropy due to layer-wise deposition and weak interlayer bonding, which compromises tensile strength perpendicular to the build direction. Surface roughness, influenced by layer height and nozzle diameter, further limits applications requiring fine finishes (Sapkota et al., 2024). However, FDM's low cost, material diversity, and compatibility with composite filaments (e.g., carbon fiber-reinforced polymers) have cemented its role in functional prototyping, educational tools, and low-volume production (Cano-Vicent et al., 2021). Recent innovations, such as dual-extrusion systems and heated chambers, aim to mitigate warping and enhance interlayer adhesion (Vyavahare & Teraiya, 2020).

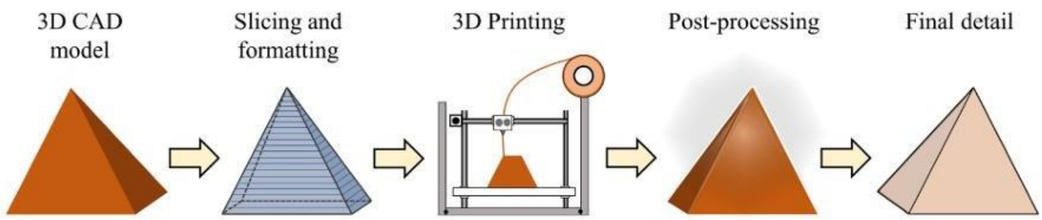

Figure 2-3 Production Stage of FDM Process
(Ab Hamid et al., 2024).

2.2.11 Infill Pattern

Infill patterns, the internal structures of FDM-printed parts, significantly influence mechanical performance, weight, and material efficiency. Standard patterns include grid, honeycomb, trihexagonal, and concentric, each offering distinct trade-offs between strength and print time. For instance, grid patterns provide isotropic strength but require longer print times, while concentric patterns align with tensile load directions, enhancing axial strength (Triawan et al., 2022).

Studies demonstrate that infill density directly correlates with tensile strength and stiffness. For example, increasing density from 15% to 75% in PLA specimens raised ultimate tensile strength by 49.6% and Young's modulus by 21.15% (Medibew & Tesfaye, 2022). However, higher densities escalate material consumption and production costs, necessitating optimization based on application requirements (Sapkota et al., 2024). Trihexagonal patterns, with 120° raster angles, exhibit superior energy absorption under dynamic loads, making them suitable for impact-resistant components. Conversely, concentric patterns minimize stress concentrations in cylindrical parts, such as pipes or biomedical scaffolds (Triawan et al., 2022).

Table 2-3 3D printing parameters
(Shaharuzaman et al., 2024).

Parameter	Value
Nozzle temperature (°C)	205–240
Bed temperature (°C)	50–100
Percent infill (%)	100, 80, 50
Printing speed (mm/s)	100
Raster angle (°)	45
Layer height (mm)	0.2
Nozzle size (mm)	0.8 & 0.4
Adhesive	Glue, Blue tape and brim
Material type	Hybrid: PLA/bamboo, PLA/wood, PLA/coconut, PLA/metal

2.2.12 Shark Fin Antenna

The shark fin antenna has emerged as a popular solution in modern automotive communication systems due to its compact design and multifunctionality. Unlike traditional whip antennas, the shark fin antenna integrates multiple communication modules such as LTE, WLAN, GPS, and satellite navigation within a single housing (Zhang, Wei, Zhang, & Li, 2024). The streamlined, aerodynamic structure of the shark fin antenna not only enhances the vehicle's aesthetic appeal but also reduces wind resistance and noise at high speeds. The growing demand for connected vehicles, driven by technologies such as vehicle-to-everything (V2X) communication and autonomous driving systems, has further underscored the importance of integrating advanced antenna solutions like the shark fin design (Kang, Kim, Lee, Kim, & Choi, 2022).

2.2.13 Function and Applications in Automotive Systems

Shark fin antennas play a crucial role in supporting multiple automotive communication needs. Their primary functions include enabling GPS navigation, supporting cellular communication (LTE, 5G), WLAN connectivity, and satellite radio reception. In addition to basic communication, shark fin antennas are critical components for modern automotive technologies such as remote keyless entry, vehicle tracking, and fleet management systems. With the expansion of IoT-based vehicular systems, shark fin antennas are increasingly designed to accommodate multiple frequency bands, ensuring compatibility with a variety of global communication standards (Saleh, Ibrahim, & Ahmed, 2020). Their integration allows for uninterrupted connectivity and data transmission, essential for advanced driver assistance systems (ADAS) and emerging autonomous vehicle platforms.

2.2.14 Design Considerations and Constraints

Designing a shark fin antenna for automotive applications involves addressing several key constraints, including size, aerodynamic performance, and multiband operation capabilities. One major challenge is achieving a compact form factor while maintaining high radiation efficiency across multiple communication bands (Haider & Jamal, 2024). Designers must ensure that the antenna does not compromise the vehicle's aerodynamics or aesthetics, while simultaneously delivering robust performance in diverse environmental conditions. Material selection and antenna placement also significantly impact signal quality and reliability.

Moreover, integration of reconfigurable antenna systems within the shark fin structure is becoming increasingly relevant to meet the evolving requirements of V2X communication (Kumar & Singh, 2023). These antennas must adapt dynamically to different communication protocols while maintaining consistent performance. Addressing electromagnetic interference (EMI) and ensuring compliance with automotive industry standards further add to the complexity of shark fin antenna design.

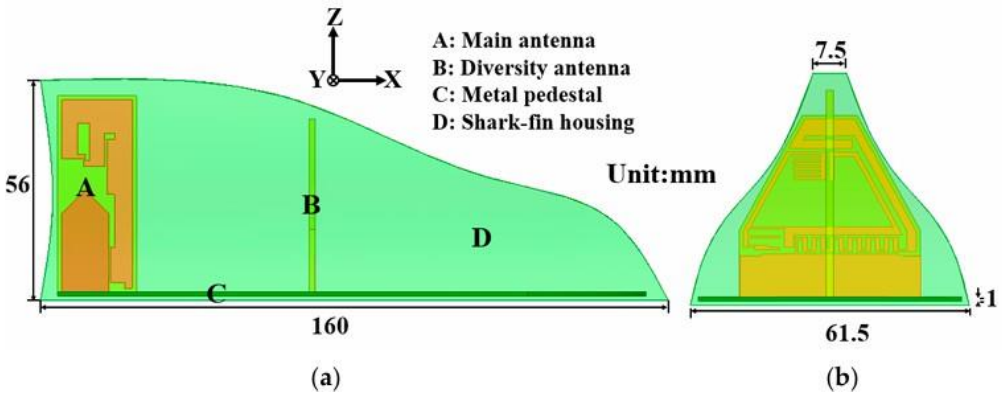

Figure 2-4 Overall structure of antenna. (a) Side view, (b) Front view.
(Zhang, Wei, Zhang, & Li, 2024)

CHAPTER 3
RESEARCH METHOD

3.1 Research Flow

The flow of the research are as follows:

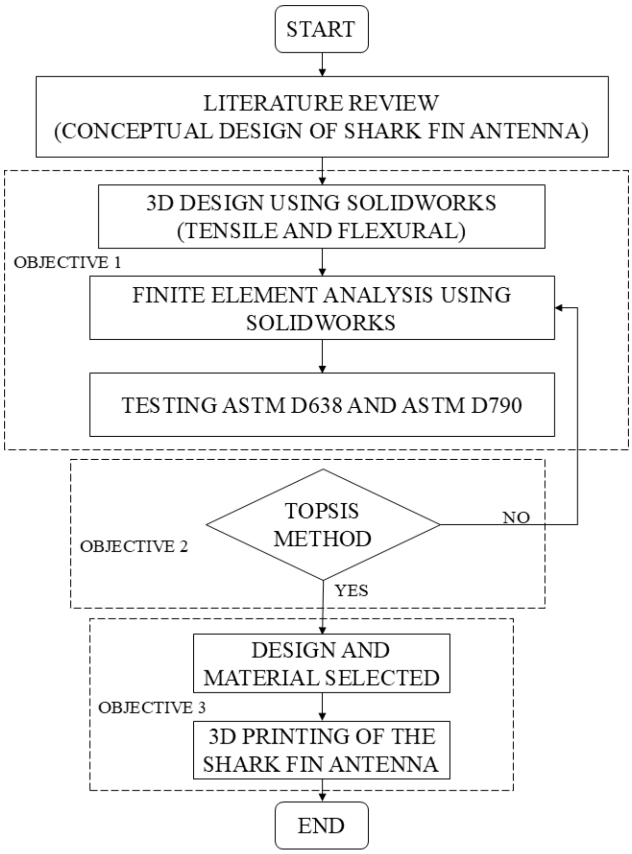

Figure 3-1 Flowchart

3.2 Equipment and Materials

1. 3D Printer

   A machine used to create specimens by printing layer-by-layer using selected filament materials, as shown in Figure 3-2.

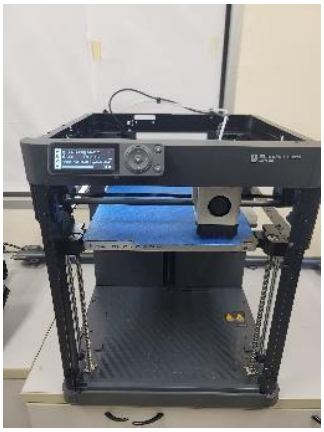

Figure 3-2 3D Printer

2. PLA/Wood Filament

   Material used for making specimens with a composition of Polylactic Acid (PLA) combined with wood fibers, as shown in Figure 3-3.

Figure 3-3 PLA/Wood Filament

3. Blue Tape

   Adhesive tape applied to the 3D printer bed to help improve print adhesion and prevent warping during specimen fabrication, as shown in Figure 3-4.

Figure 3-4 Blue Tape

4. Tensile Testing Machine

   INSTRON 8872 A device used to measure the tensile strength and elongation of a specimen by applying a uniaxial pulling force, as shown in Figure 3-5.

Figure 3-5 Tensile Testing Machine

5. Flexural Testing Machine

   INSTRON 5585 A device used to measure the flexural strength and deflection of a specimen by applying a bending force, as shown in Figure 3-6.

Figure 3-6 Flexural Testing Machine

3.3 Conceptual Design

At this point, the conceptual design of the shark fin antenna was designed to satisfy practical, aesthetic, and performance criteria for contemporary vehicles. The design process drew inspiration from many commercially available shark fin antennas, aiming to modify existing designs to enhance aerodynamic performance, structural integrity, and installation convenience for the specified research objectives.

A comprehensive evaluation of commercial shark fin antennas was conducted to ascertain current design attributes, materials, and installation techniques. Products from renowned automotive brands were analysed for their aerodynamic properties, geometric configurations, and integration with vehicle structures. This benchmarking elucidated effective components, including seamless surface transitions and resilient mounting procedures, which were deemed for subsequent adaptation and enhancement. Each concept as shown in Figure 3-7, 3-8, 3-9 were modeled using Solidworks software to visualize form, fit, and approximate volume. Strengths and limitations of each design were analyzed, particularly in terms of aerodynamic flow, internal housing capacity, and manufacturability.

3.3.1 Conceptual Design 1

Figure 3-7 Conceptual Design 1
(Taoglas, 2019)

Conceptual Design 1 is based on the Taoglas MA1044 4-in-1 shark fin antenna (Taoglas, 2019). This concept adopts a multi-functional approach by integrating four different antenna systems within a single housing: GNSS, Wi-Fi, SDARS, and AM/FM. The housing is designed using a robust ASA+PC material with UV stabilizer, ensuring durability and weather resistance under outdoor conditions. The enclosure measures approximately 183.6 mm × 80.9 mm × 77.3 mm, providing sufficient space for the internal antenna elements. The internal configuration uses FAKRA-coded coaxial connections to ensure secure and standardized installation. Conceptual design 1 aims to achieve high performance in signal reception across multiple frequency bands while maintaining a compact and aerodynamic profile suitable for permanent vehicle roof mounting.

3.3.2 Conceptual Design 2

Figure 3-8 Conceptual Design 2
(Junecarp)

Conceptual design 2 is inspired by a commercial from Junecarp Shark Fin Antenna. Unlike Conceptual design 1, this design focuses on a more minimalist configuration, housing a single AM/FM antenna within a smaller, cleaner shell. The streamlined shape minimizes aerodynamic drag while preserving a contemporary look that blends with modern vehicle styling. Its relatively compact footprint is ideal for vehicles where integration with other telematics systems is not necessary. The glossy white surface combined with a black rubber base offers a stylish yet practical solution for typical passenger vehicles. This concept emphasizes ease of manufacturing and lower cost compared to multi-functional antennas, making it attractive for manufacturers targeting basic connectivity functions.

3.3.3 Conceptual Design 3

Figure 3-9 Conceptual Design 3
(Taoglas, 2024)

Conceptual design 3 takes inspiration from the Taoglas MA1290 Raptor III 7-in-1 Shark Fin antenna (Taoglas, 2024). This high-performance concept integrates an advanced suite of antenna systems, including GNSS (GPS/GLONASS/BeiDou/Galileo), dual 5G/4G MIMO, dual-band Wi-Fi MIMO, VHF/UHF/LMR, and active AM/FM, all within a single compact unit. The antenna is designed with two detachable whip antennas to accommodate varying frequency applications, including TETRA and public safety bands. The robust enclosure, made from UV-resistant PC, is rated IP67 for water and dust ingress, making it ideal for both commercial and emergency vehicle deployments. Its dimensions are approximately 191 mm × 95.7 mm × 98.3 mm (excluding whip), offering a slightly larger footprint to house its complex internal architecture. Cable assemblies are 3 meters long with SMA, RP-SMA, and Mini UHF connectors, providing flexibility in installation. This concept aims to serve mission-critical communication systems and connected mobility applications by offering broad frequency support, modular whip options, and reliable high-efficiency signal transmission across all integrated channels.

3.4 Design Evaluation

When evaluate the design, the simulation focus on assessing factors such as pressure distribution, flow trajectories. To evaluate those properties using Solidworks flow simulation, the drag coefficient, drag force and frontal area of the shark fin antenna need to be defined. The goal no 1 is specified on drag force that been automatically calculated using software when the simulation run based on the input parameter as shown in table 3.2. The equation as stated in equation (1) are used to obtain goal no 2 which is the coefficient of drag. The frontal area of each design is retrieved as in table 3.1 to satisfy the equation. Goal no 3 is specified to pressure in the surface area on which direction of the flow past. The velocity applied is 25.04 m/s or equal to 90.15 km/h, based on real vehicle data (Hu et al., 2024).

$$C_d = 2F_d / (\rho \times V^2 \times A) \tag{1}$$

Where,

F_d: Drag Force, A: Frontal Area, ρ: Fluid density, V: velocity,

C_d: Drag coefficient

Table 3-1 Input parameters of simulation using Solidworks Flow

Thermodynamic Parameter	
Pressure (Pa)	101325
Temperature (K)	293.2
Velocity Parameter	
Velocity in X/Y/Z direction (m/s)	25.04 (Hu et al., 2024)

The design with the lower pressure distribution, most constant and even velocity distribution and lower drag force will be considered as best design.

3.5 Printing specimen

The printing parameter configuration to build the specimen for the testing of the material using fused deposition modelling (FDM) filament by using Bambu lab P1P model is in Figure 3-10 and is described in Table 3.3

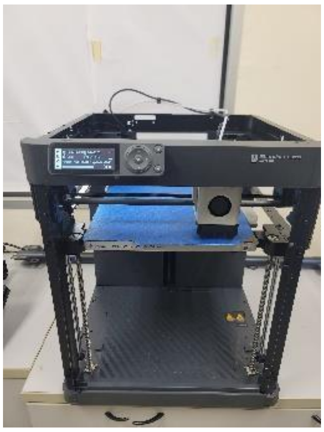

Figure 3-10 Bambu Lab P1P

Table 3-2 Description of printing parameters

Parameter	Value
Nozzle temperature (°C)	220
Bed temperature (°C)	70
Percent infill (%)	50, 75, 100
Printing speed (mm/s)	100
Infill Direction (°)	45
Layer height (mm)	0.2
Nozzle size (mm)	0.4
Adhesive	Blue tape and brim
Material type	PLA/wood

The printing procedure started with PLA/wood as the material, and a total of 15 specimens were produced using a 3D printer from Bambu Lab P1P. According to ASTM D638 and ASTM D790 specifications, the specimen is printed in rectangular and dogbone forms, respectively. Additionally, each specimen is printed in five pieces with 50%, 75%, and 100% infill using a 0.4mm nozzle, as specified in Table 3.5. This is done in order to assess the specs. With a 1.75 mm filament, the nozzle's temperature settings fall between 220°C. The specimen was supported by the brim, an adhesive that is applied during the printing process. The infill pattern that was selected is a rectilinear pattern layer configuration, which comprises of lines and offers extra support for the plate adhesion of the specimens throughout the printing process, to pursue a direct, economical solution that maintains strong mechanical performance and consistent behavior under diverse stress conditions (Cojocaru & Miclosina, 2020). Brims serve the twin purposes of avoiding warping and improving bed adhesion. In addition, brim and 3D blue tape can be used to create additional support for the bed adhesion. Figures 3.6 shows the printed specimens for tensile and flexural testing.

(a)

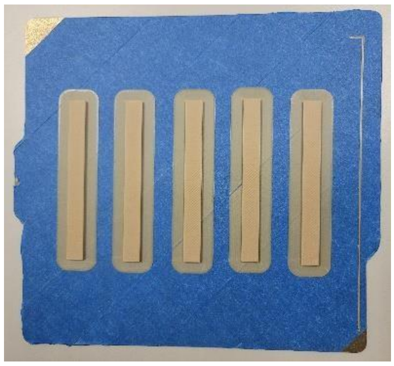

(b)

Figure 3-11 Printed specimens (a) for tensile test
(b) for flexural test

3.6 Tensile Test

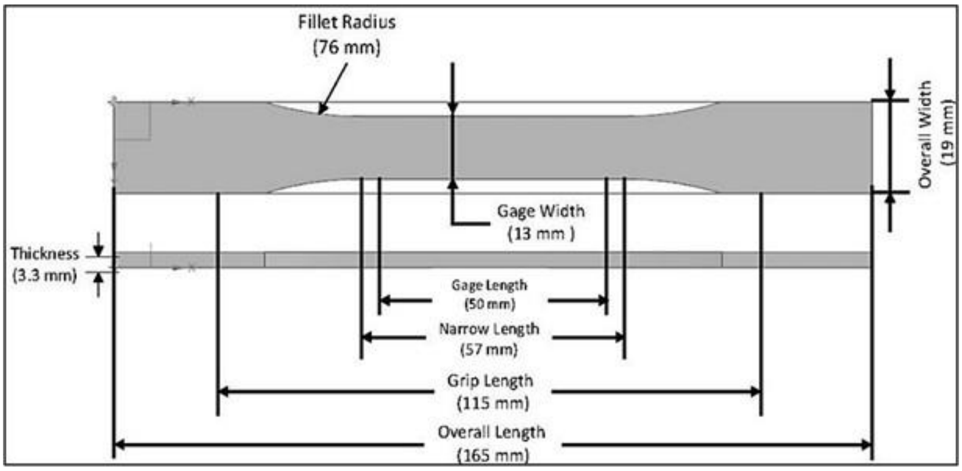

Figure 3-12 Dimension of Tensile Test based on ASTM D638
(Sulaiman et al., 2025)

The tensile testing adheres to the ASTM D638 Type I standard. According to ZwickRoell, ASTM D638 type I as the preferred specimen for rigid plastics, ensuring alignment with standardized characterization protocols. The filament examined is 1.75mm PLA/Wood, and tensile testing will be conducted on a total of fifteen specimens, with infill percentages of 50%, 75%, and 100%. The specimen, as seen in Figure 3.7, will be constructed with a thickness of 3.3 mm, an overall length of 165 mm, and an overall width of 19 mm.

The model is tested using the INSTRON 8872 universal testing equipment. After aligning the specimen's longitudinal axis, it is dragged across the crosshead at a rate of 2 mm per minute based on ASTM International (2015), to have optimal data resolution and accuracy. The specimens are progressively stressed until they break under uniaxial tensile strain using a tension testing machine. At room temperature, the maximum load that may be applied during this procedure is 1,5 kN. The specimen is positioned as shown in Figure 3-13.

Figure 3-13 Placement of tensile specimen

3.7 Flexural Test

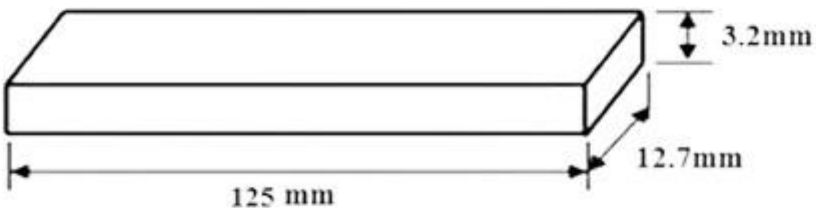

Figure 3-14 Dimension of Flexural Test based on ASTM D790 (Sulaiman et al., 2025)

The flexural test, commonly referred to as the bending test, was done in accordance with ASTM D790, and the specimen dimensions are illustrated in Figure 3-14. The testing method assesses the flexural characteristics of both reinforced and unreinforced plastics, high-modulus composites, and electrical insulation materials. The specimens utilised are normal PLA/Wood 1.75mm filament, which will be manufactured into five specimens including varying infill percentages, with 50%, 75% and 100% infill. This will result in a total of 15 specimens being tested.

The universal testing machine, model INSTRON 5585, is the one in use. The load orientation for the 3-point bend test type was parallel to the direction of the specimen. With crosshead speed is set at 2 mm/min. The specimen will be subjected to load until it fractures or bends to its maximum. The span-to-depth ratio for specimen placement support is 16:1, which is the norm. The specified 3.2 mm thickness ratio resulted in a 51.2 mm support span. Figure 3-15 shows where the specimen is located. A material is considered to have failed in accordance with the

ASTM D790 standard if it does not fracture or yield on the specimen's exterior within the 5.0% strain limit (ASTM, 2017).

Figure 3-15 Placement of flexural specimen

3.8 Technique for Order of Preference by Similarity to Ideal Solution (TOPSIS) Method

The mechanical characteristics data from testing and the information acquired for three conceptual designs will be rated using the TOPSIS approach to ascertain the score ranking of the optimal material and design for the superior shark fin antenna, provides a clear and easily interpretable ranking of alternatives, facilitating decision making and communication (Sahoo & Goswami, 2023). The fundamental procedures of the TOPSIS approach, including its formula and computation, the steps are as follows (Behzadian *et al.*, 2012):

Step 1: Construct normalized decision matrix.

$$r_{ij} = \frac{X_{ij}}{\sqrt{\sum X_{ij}^2}} \text{ for i = 1,…, m; j = 1,.., n} \quad (2)$$

where X_{ij} and and $r_{ij}$are original and normalized score of decision matrix.

Step2: Construct the weighted normalized decision matrix.

$$v_{ij} = w_j \, r_{ij} \quad (3)$$

Where w_j is the weight for j criterion.

Step 3: Determine the positive ideal and negative ideal solutions.

$$V^{+} = \{v_1, \ldots, v_n\} \quad \text{Positive ideal solution} \quad (4)$$

$$V^{-} = \{v_1, \ldots, v_n\} \quad \text{Positive ideal solution}$$

$$\text{Where } V_j = \{\max (v_{ij}) \text{ if } j \in J;\ \min (v_{ij}) \text{ if } j \in J'\}$$

$$V^{-} = \{v_1', \ldots, v_n'\} \quad \text{Negative ideal solution} \qquad (5)$$

Where $v' = \{min\ (v_{ij})\ if\ j\ \in J;\ max\ (v_{ij})\ if\ j \in J'\}$

Step 4: Calculate the separation measures each alternative.

$$Si^{+} = [\sum (v_i - v_{ij})^2\ ]^{1/2} \quad i = 1, \ldots, m \qquad (6)$$

Similarly, the separation from the negative ideal alternative is:

$$Si^{-} = [\sum (v_i - v_{ij})^2\ ]^{1/2} \quad i = 1, \ldots, m \qquad (7)$$

Step 5: Calculate the relative closeness to the ideal solutio

$$C_i = S'_i / (S_i + S'_i)\ ,\ 0 < C_i < 1 \qquad (8)$$

Alternative which closes to 1 is selected.

CHAPTER 4
RESULTS AND DISCUSSION

4.1 Design Results

4.1.1 Flow Trajectories

The evaluation of the three proposed designs for the shark fin antenna focused on analyzing flow trajectories, illustrating the direction and velocity of airflow around each design. The trajectories, illustrated by streamlines colored to represent velocity magnitude, offered essential insights into the airflow dynamics around and interaction with the antenna's surfaces. However, in this study, there are variations in color.

Specify the maximum and minimum when the airflow approaches the antenna surfaces. This is attributable to the variation in axes throughout the generation of conceptual designs. The research identified regions of wake creation, resistance, or streamlined airflow by examining the patterns and fluctuations in airflow. The flow trajectories for each design are depicted in the table 4.1.

Table 4-1 Flow trajectories for conceptual designs

Design	Flow Trajectory	Velocity (m/s)
Conceptual Design 1	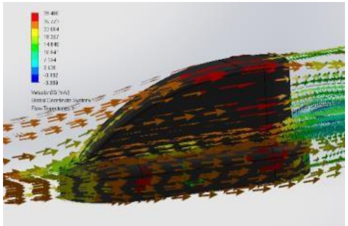	Max: 29.480
Conceptual Design 2		Max: 29.921
Conceptual Design 3	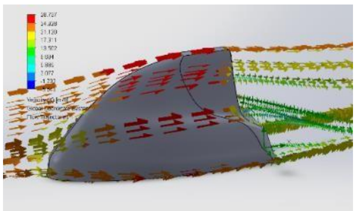	Max: 28.737

The results presented in the table 4.1 provides insights into the flow trajectory and maximum velocity for each shark fin antenna design, as determined by flow simulation analysis. The flow trajectories, visualized through colored streamlines, illustrate how air moves around and interacts with each antenna surface.

Design 2 exhibits the highest maximum velocity of 29.921 m/s, indicating more attached and streamlined airflow; yet, the drag force simulation results reveal that Design 3 possesses the lowest drag force among the designs. Design 3's diminished maximum velocity of 28.737 m/s is indicative of less aerodynamic resistance, as demonstrated by its enhanced drag force performance. This underscores that although increased maximum velocity may suggest smoother airflow, the overall aerodynamic efficiency is more accurately reflected by the drag force, with lower values being desirable.

The flow patterns indicate that Design 2 facilitates continuous airflow; nevertheless, the modest wake development and increased drag force imply that this does not inherently result in the lowest resistance. Conversely, Design 3, although possessing a marginally reduced maximum velocity, has superior flow separation management and little wake, culminating in the lowest drag force. Design 1 has an intermediate position regarding both velocity and drag force levels.

Consequently, based on the analysis of flow trajectory and drag force outcomes, Design 3 is identified as the most aerodynamically efficient shark fin antenna, providing an optimal equilibrium between airflow dynamics and reduced resistance.

4.1.2 Pressure Distribution

The assessment of the three proposed designs for the shark fin antenna entailed a comprehensive investigation of pressure distribution over their surfaces. This simulation facilitated the comprehension of how fluctuations in air pressure affected the aerodynamic efficacy of each design. The identification of high-pressure zones signifies parts where air resistance may obstruct smooth airflow, whereas the low-pressure regions denote sections favorable for a more streamlined and unobstructed air flow.

Table 4.2 indicates that the surface pressure values among the various shark fin antenna designs exhibit minimal variances. This signifies a uniform aerodynamic pressure distribution across the proposed designs. Despite minor discrepancies in pressure measurements, the general resemblance indicates that the interaction of airflow with the antenna surfaces is predominantly consistent. Thus, the surface pressure results indicate a similar degree of aerodynamic effectiveness regarding pressure distribution across all assessed shark fin antenna designs. The highest pressure among these designs is 101829.87 Pa, which is occurred in design 2 and the best design based on surface pressure simulation is design 1 with value of pressure 101644.52 Pa.

Table 4-2 Pressure distribution for all conceptual design

Design	Pressure Distribution	Pressure (Pa)
Conceptual Design 1	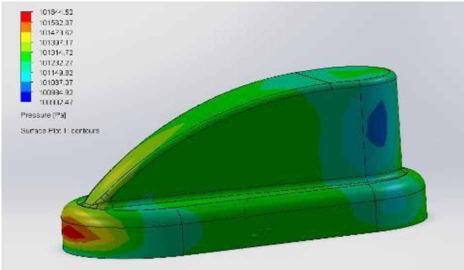	Max: 101644.52
Conceptual Design 2	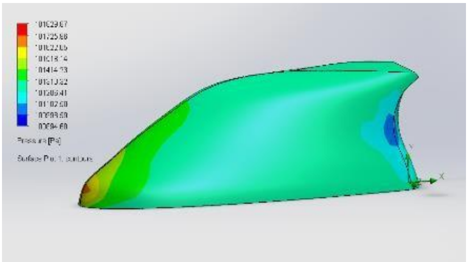	Max: 101829.87
Conceptual Design 3	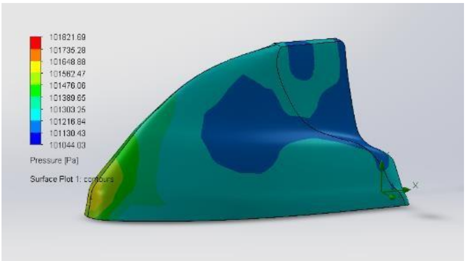	Max: 101821.69

4.1.3 Aerodynamic Properties

Three conceptual designs that have been developed are presented in Table 4.4. The data comprise properties that may affect the aerodynamic performance of the shark fin antenna, that are affected by its frontal area as presented in Table

4.3. The results are presented in bar charts to facilitate a clear comparison of the designs for their individual aerodynamic features, as depicted in Figures 4.1, 4.2, and 4.3.

Table 4-3 Frontal area of each design

Design	Frontal Area (mm^2)
Design 1	4775.01
Design 2	4634.40
Design 3	4208.88

Table 4-4 Result for aerodynamic properties

Design	Drag Force (N)	Coefficient Drag (N)	Surface Pressure (Pa)
Conceptual Design 1	0.563	0.222	101644.52
Conceptual Design 2	0.602	0.237	101829.87
Conceptual Design 3	0.457	0.215	101821.69

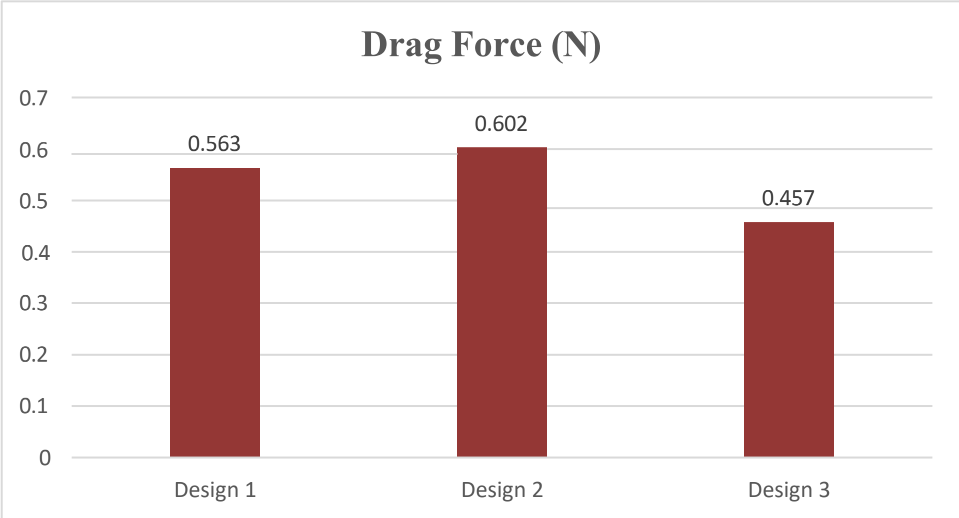

Figure 4-1 Drag Force

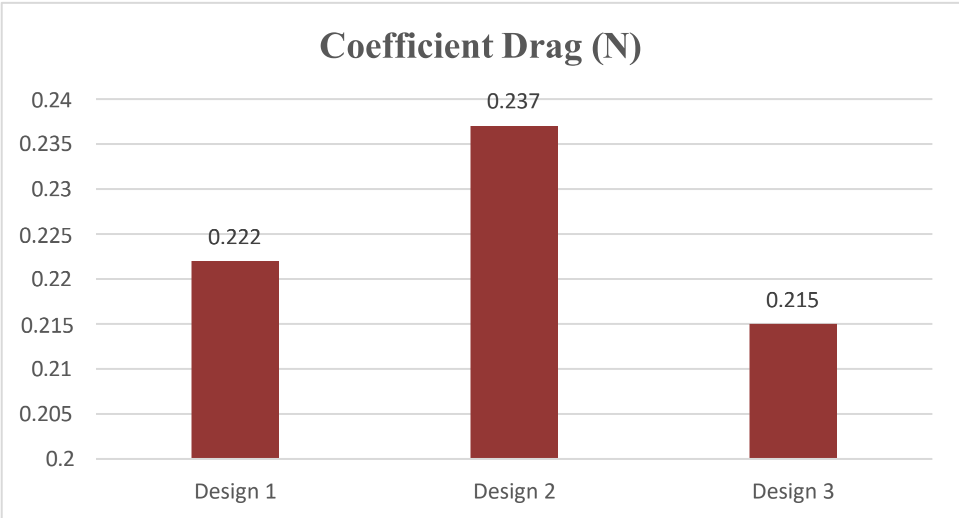

Figure 4-2 Coefficient Drag

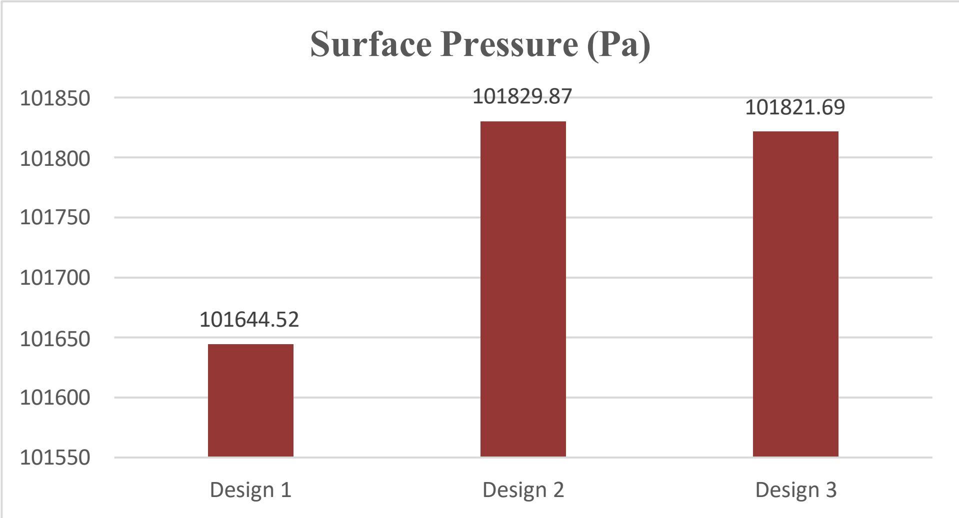

Figure 4-3 Surface Pressure

In the context of the shark fin antenna, drag force represents the resistance encountered by the antenna as air flows past it. According to Figure 4-1, Design 3 exhibits the lowest drag force at 0.457 N, indicating it experiences the least resistance among the three designs. In comparison, Design 2 has the highest drag force at 0.602 N, while Design 1 falls in between at 0.563 N. This suggests that Design 3 is the most aerodynamically efficient, as lower drag force generally corresponds to reduced energy loss and improved performance

The coefficient of drag quantifies how streamlined each antenna design is against airflow. As shown in Figure 4-2, Design 3 again demonstrates the lowest coefficient of drag at 0.215, signifying a more aerodynamically favorable shape. Design 2 records the highest value at 0.237, and Design 1 is moderate at 0.222. A lower coefficient of drag indicates that Design 3 is better optimized to minimize resistance and enhance airflow, making it the most effective design in terms of aerodynamic streamlining.

Surface pressure measures the distribution of air pressure acting on the antenna's surface in the direction of airflow. Figure 4-3 reveals that Design 1 experiences the lowest surface pressure at 101644.52 Pa, while Designs 2 and 3 have higher values at 101829.87 Pa and 101821.69 Pa, respectively. Although Design 1 has the lowest surface pressure, the differences among the designs are relatively small. This suggests that, while surface pressure varies, its impact on overall aerodynamic performance is less pronounced compared to drag force and drag coefficient.

Overall, these results indicate that Design 3 offers the best aerodynamic characteristics among the evaluated shark fin antenna designs, with the lowest drag force and drag coefficient, contributing to enhanced efficiency and reduced resistance in practical applications.

4.2 Testing Results

4.2.1 Tensile Result

The tensile test results for the NFC filament-PLA/Wood specimen are presented in Table 4.4. The data comprises results of various printing parameter properties that may affect the material's integrity. The data are illustrated in a bar chart to facilitate a clear comparison of the various parameters influencing their mechanical properties, as depicted in Figure 4-4 and 4-5.

Table 4-5 Result for tensile test

Material - Infill Density	**Average Tensile Strength (MPa)**	**Tensile Young Modulus (GPa)**
PLA / Wood – 50%	25.828	1.173
PLA / Wood – 75%	27.042	1.245
PLA / Wood – 100%	37.462	1.663

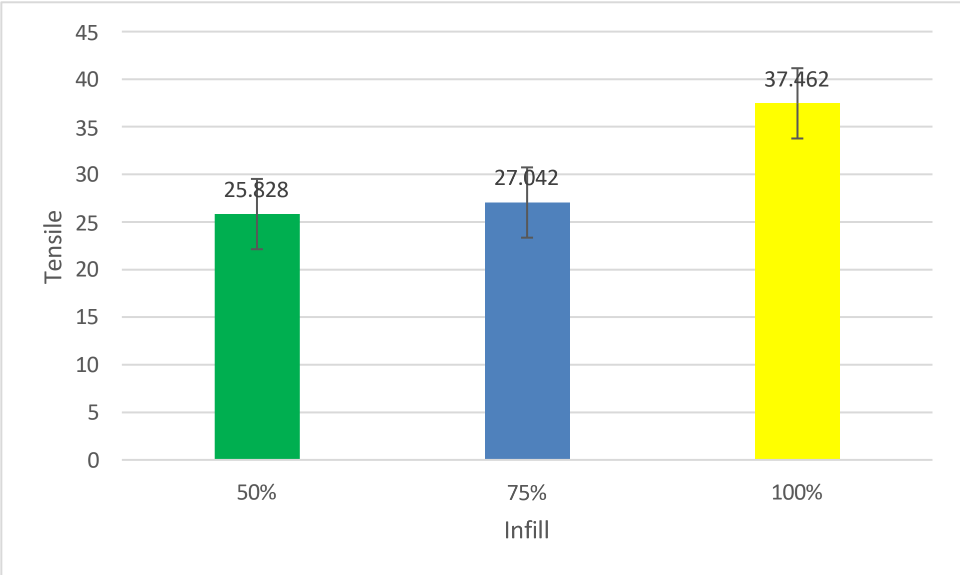

Figure 4-4 Tensile Strength for PLA/Wood with different infill density

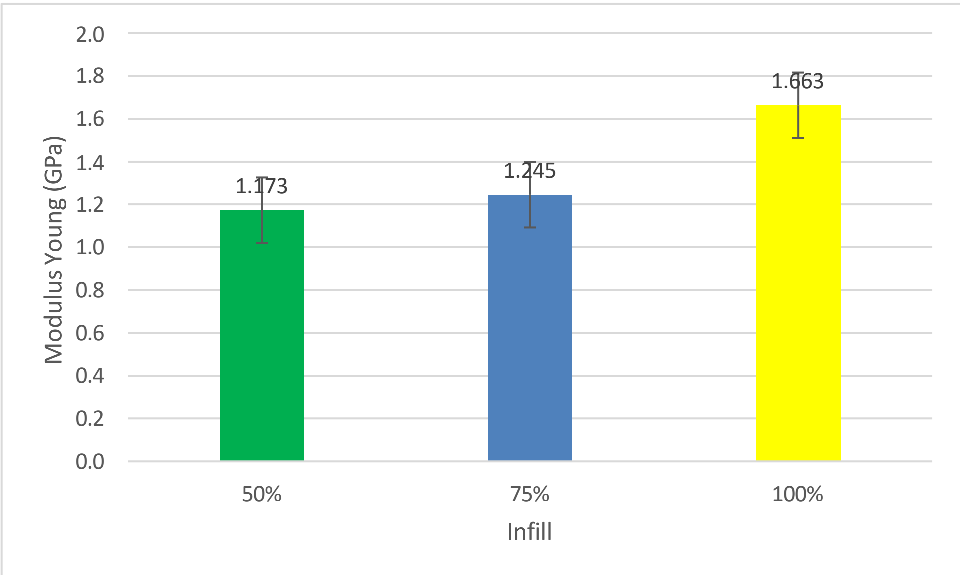

Figure 4-5 Young Modulus for PLA/Wood with different infill density

The experimental results show a progressive increase in tensile strength as infill density increases from 50% to 100%. The specimens printed with 50% infill density achieved a tensile strength of 25.828 MPa, representing the baseline performance for the lowest density configuration tested. This value provides insight into the minimum mechanical performance that can be expected from PLA/Wood composites when material efficiency and printing speed are prioritized over maximum strength.

The intermediate infill density of 75% demonstrated a moderate improvement in tensile strength, reaching 27.042 MPa. This represents approximately an 8% increase over the 50% infill configuration, indicating that even modest increases in infill density can yield measurable improvements in mechanical performance. This intermediate configuration offers a balance between material usage, printing time, and mechanical properties, making it potentially suitable for applications where moderate strength requirements must be met while maintaining reasonable production efficiency.

The highest tensile strength was achieved with 100% infill density, reaching 37.462 MPa. This represents a substantial 47% improvement over the 50% infill specimens and a 36% increase compared to the 75% infill configuration. The significant jump in performance between 75% and 100% infill suggests that complete material densification provides disproportionate benefits in terms of tensile strength, likely due to the elimination of internal voids and the creation of a more continuous load transfer mechanism throughout the specimen cross-section.

The elastic modulus values demonstrate a consistent upward trend corresponding to increased infill density, similar to the tensile strength behavior observed1. The 50% infill specimens exhibited a Young's modulus of 1.173 GPa, establishing the baseline elastic performance for the composite material. This relatively low stiffness value reflects the presence of internal voids and reduced material continuity inherent in lower-density infill patterns.

The 75% infill configuration showed improved elastic properties with a Young's modulus of 1.245 GPa. This represents approximately a 15% increase over the 50% infill specimens, indicating that the additional material deposition in the intermediate density configuration contributes meaningfully to overall structural stiffness. The improvement suggests that the 75% infill pattern provides better load distribution and stress transfer mechanisms compared to the sparser 50% configuration.

The 100% infill specimens achieved the highest Young's modulus value of 1.663 GPa. This represents a 42% improvement over the 50% infill baseline and a 24% increase compared to the 75% infill configuration. The substantial improvement in elastic modulus with complete infill reflects the creation of a more homogeneous material structure that approaches the properties of a solid composite material rather than a cellular or porous structure.

According to Triawan et al. (2022), higher infill densities in 3D-printed PLA specimens significantly enhance tensile strength and Young's modulus by reducing internal porosity and improving material continuity, leading to more uniform stress distribution under load. This aligns with experimental evidence showing 75% infill density specimens achieving 35.41 MPa tensile strength compared to 26.08 MPa at 15% density, demonstrating a 35.7% strength improvement through increased material consolidation.

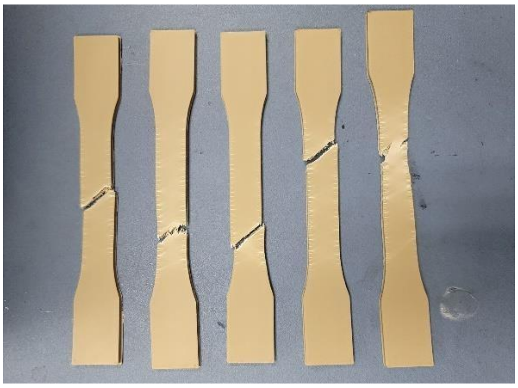

(a)

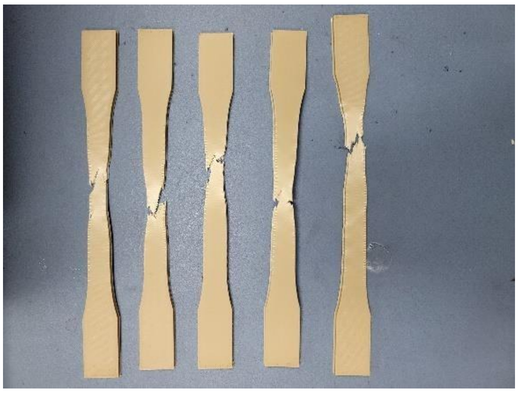

(b)

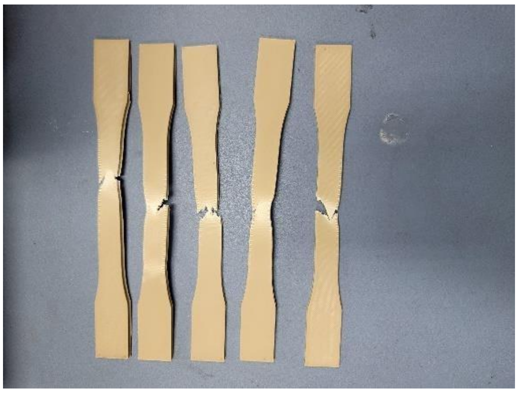

(c)

Figure 4-6 Specimen after tensile test

(a) 50% infill (b) 75% infill (c) 100% infill

4.2.2 Flexural Test

Comparable to the tensile test, the NFC filament-PLA/Wood specimens subjected to the three-point bending test are presented in Table 4.5. The data comprises results from various printing parameters. The results are presented in bar charts to provide a clear comparison of the many parameters influencing their mechanical characteristics, as seen in Figures 4-7 and 4-8.

Table 4-6 Result of Flexural Test

Material - Infill Density	Average Flexural Stress (MPa)	Modulus of Elasticity (GPa)
PLA / Wood – 50%	48.890	2.231
PLA / Wood – 75%	58.791	2.517
PLA / Wood – 100%	65.187	2.694

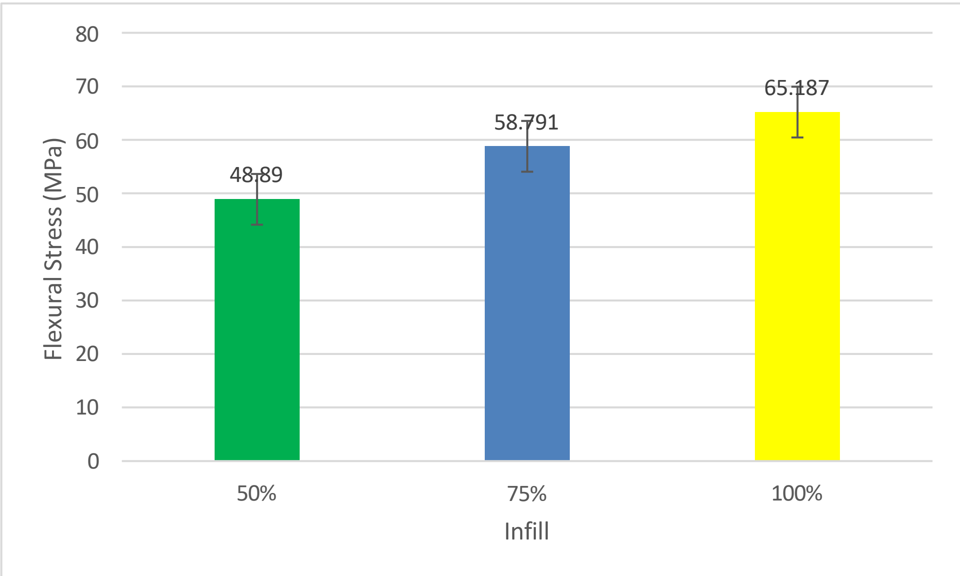

Figure 4-7 Flexural Stress for PLA/Wood with different infill density

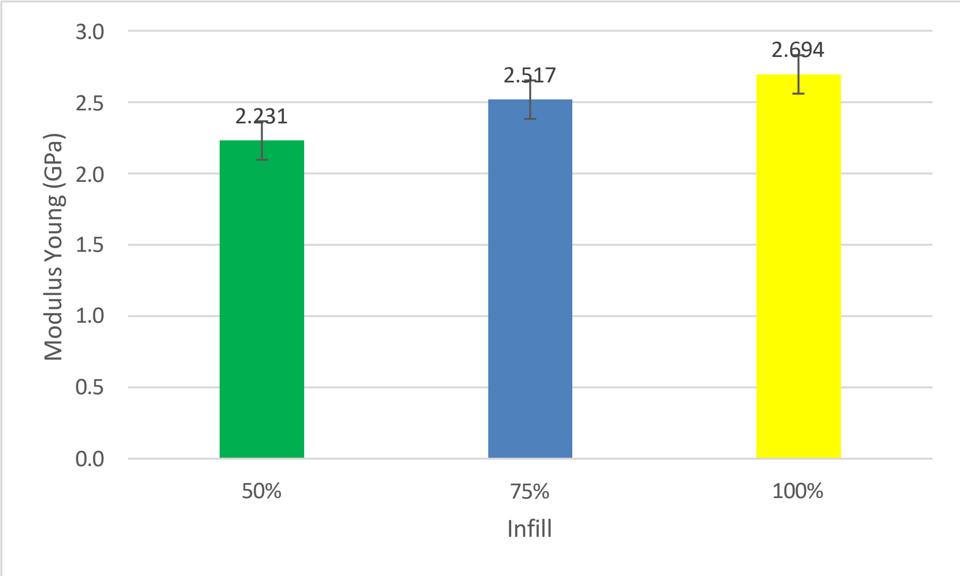

Figure 4-8 Modulus of Elasticity for PLA/Wood with different infill density

Based on the chart in Figure 4.7, the specimen printed with 100% infill density achieved the highest flexural strength with a value of 65.187 MPa, while the specimen with 50% infill density recorded the lowest performance at 48.89 Mpa. The intermediate infill density of 75% demonstrated a flexural strength of 58.791 Mpa, positioning it between the maximum and minimum values obtained. This represents a substantial 34% improvement in flexural strength when comparing the 100% infill specimens to the 50% infill baseline, indicating the significant influence of infill density on bending resistance.

The progressive ©ncrease in flexural strength correlates directly with the increased material density within the specimen structure. The 100% infill configuration creates a more solid and continuous internal architecture that provides superior resistance to bending loads compared to the partially filled structures. The 75% infill specimens showed a 20% improvement over the 50%

infill configuration, demonstrating that even moderate increases in material density can yield meaningful enhancements in flexural performance.

The modulus of elasticity measurements, as shown in Figure 4.8, reveal a similar trend to the flexural strength results. The specimens printed with 100% infill density exhibited the highest elastic modulus of 2.694 Gpa, while those with 50% infill density showed the lowest value at 2.231 Gpa. The 75% infill specimens achieved an intermediate modulus of elasticity of 2.517 Gpa. The modulus of elasticity quantifies the material's stiffness and resistance to elastic deformation under applied bending loads, serving as an indicator of the material's structural rigidity.

The relationship between infill density and elastic modulus follows a consistent upward trend, with the 100% infill specimens showing approximately 13% higher stiffness compared to the 50% infill configuration. This improvement in elastic properties reflects the enhanced material continuity and reduced internal porosity achieved through higher infill densities. The 75% infill specimens demonstrated an 8% increase in elastic modulus over the 50% baseline, indicating that the intermediate density provides measurable improvements in structural stiffness.

According to Triawan et al. (2022), higher infill densities in 3D-printed PLA specimens significantly enhance tensile strength and Young's modulus by reducing internal porosity and improving material continuity, leading to more uniform stress distribution under load. This phenomenon extends to flexural properties, where increased infill density creates a more homogeneous material structure that better distributes bending stresses throughout the specimen cross-section. The reduced void content in higher infill density specimens eliminates stress concentration points that could otherwise serve as failure initiation sites under flexural loading.

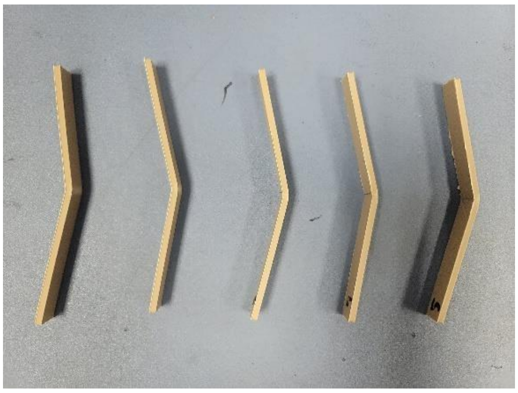

(a)

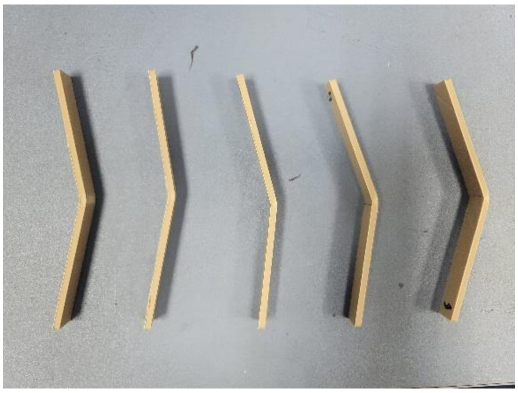

(b)

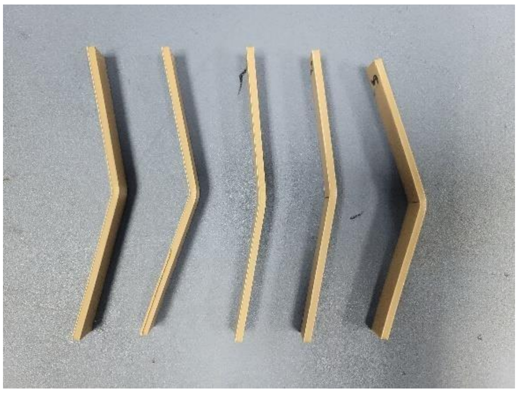

(c)

Figure 4-9 Specimen after flexural test
(a) 50% infill (b) 75% infill (c) 100% infill

4.2.3 Technique for Order of Preference by Similarity to Ideal Solution (TOPSIS) for Conceptual Design

The TOPSIS method was employed to select best design. Aerodynamic properties data of each design were utilized in Table 4.6 for this method's calculations. The resulting Ci values were obtained through TOPSIS to rank from the best to worst design.

Table 4-7 Data of aerodynamic properties of each design

Design	Drag Force (N)	Coefficient Drag (N)	Surface Pressure (Pa)
Design 1	0.563	0.222	101644.52
Design 2	0.602	0.237	101829.87
Design 3	0.457	0.215	101821.69

i. First step involves the determination decision matrix ,A as in equation (2)

$$A = \frac{x_{ij}}{\sqrt(\sum x_{ij})}$$

Design	Drag Force (N)	Coefficient Drag (N)	Surface Pressure (Pa)
Design 1	0.563	0.222	101644.52
Design 2	0.602	0.237	101829.87
Design 3	0.457	0.215	101821.69
A	0.942	0.389	176262.84

ii. Next, weighted normalized decision matrix are constructed as in equation (3).

$$v_{ij} = w_i \, r_{ij}$$

Design	Drag Force (N)	Coefficient Drag (N)	Surface Pressure (Pa)
Design 1	0.598	0.571	0.576664
Design 2	0.639	0.609	0.577716
Design 3	0.485	0.553	0.577670
Weightage	0.333	0.333	0.334

iii. Step 3 involves the determination of the positive ideal and negative ideal solutions as in equation (4) and (5).

$V^+ = \{v_1, \ldots, v_n\}$ Positive ideal solution

$V^- = \{v_1', \ldots, v_n'\}$ Negative ideal solution

Design	Drag Force (N)	Coefficient Drag (N)	Surface Pressure (Pa)
Design 1	0.199	0.190	0.192606
Design 2	0.213	0.203	0.192957
Design 3	0.161	0.184	0.192942
V+ (best)	0.161	0.184	0.192606
V- (worst)	0.213	0.203	0.192957

iv. The data then being calculated by separation measures for each alternative as in equation (6) and (7).

$$Si^{+} = \left[\sum (v_i - v_{ij})^2\right]^{1/2} \quad i = 1,\ldots,m$$

Similarly, the separation from the negative ideal alternative is:

$$Si^{-} = \left[\sum (v_i - v_{ij})^2\right]^{1/2} \quad i = 1,\ldots,m$$

v. Lastly, the data is calculated by the relative closeness to the ideal solution as in equation (8).

$$C_i = S'_i / (S_i + S'_i) \ , \ 0 < C_i < 1$$

Alternative which closes to 1 is selected.

Table 4-8 Result of TOPSIS method for design selection

Design	$\boldsymbol{Si^{+}}$	$\boldsymbol{Si^{-}}$	**Performance Score**		**Rank**
			$(\boldsymbol{Si^{+}}) + (\boldsymbol{Si^{-}})$	$\boldsymbol{C_i}$	
Design 1	0.0380	0.0191	0.0571	0.334	2
Design 2	0.0524	0	0.0524	0.000	3
Design 3	0.0003	0.0554	0.0557	0.995	**1**

Based on table 4.7, the design with the highest Ci value among the others is design 3 with highest Ci 0.995. In contrast, design 2 ranks at the lowest with value of Ci 0.00. As a result, design 3 is selected and been used to fabricate the actual product which shark fin antenna by 3D printing.

4.2.4 Technique for Order of Preference by Similarity to Ideal Solution (TOPSIS) for Material

The TOPSIS approach was utilized to identify the optimal material. The mechanical characteristics data for each NFC filament are included in Table 4.8 for the calculations of this method. The resultant Ci values were derived using TOPSIS to rank the materials from best to worst for the specified design, which is design 3.

Table 4-9 Data of mechanical properties NFC filaments

Material	Tensile Strength (MPa)	Young Modulus (MPa)	Flexural Stress (MPa)	Modulus of Elasticity (MPa)	Cost (RM)
PLA/Wood 1	37.46	1663.000	65.187	2694.000	72.00
PLA/Wood 2	36.62	5341.530	37.180	1182.400	79.00
PLA/Coconut	30.70	5203.030	39.360	1461.770	152.94
PLA/Bamboo	32.83	4879.130	41.040	1071.330	156.90

I. The calculation for step 1 is calculated as equation (2) which determination of decision matrix.

$$A = \frac{x_{ij}}{\sqrt{(\sum x_{ij})}}$$

Material	Tensile Strength (MPa)	Young Modulus (MPa)	Flexural Stress (MPa)	Modulus of Elasticity (MPa)	Cost (RM)
PLA/Wood 1	37.460	1663.000	65.187	2694.000	72.00
PLA/Wood 2	36.620	5341.530	37.180	1182.400	79.00
PLA/Coconut	30.700	5203.030	39.360	1461.770	153.00
PLA/Bamboo	32.830	4879.130	41.040	1071.330	156.90
	69.026	9065.04	94.155	3455.463	243.83

II. Next, the calculation for step 2 is calculated as in equation (3) which constructing the weighted normalized decision matrix.

$$v_{ij} = w_i \, r_{ij}$$

Material	Tensile Strength (MPa)	Young Modulus (MPa)	Flexural Stress (MPa)	Modulus of Elasticity (MPa)	Cost (RM)
PLA/Wood 1	0.5427	0.1835	0.6923	0.7796	0.2953
PLA/Wood 2	0.5305	0.5892	0.3949	0.3422	0.3241
PLA/Coconut	0.4448	0.5740	0.4180	0.4230	0.6273
PLA/Bamboo	0.4756	0.5382	0.4359	0.3100	0.6436
Weightage	0.200	0.200	0.200	0.200	0.200

III. Step 3 involves the determination of the positive ideal and negative ideal solutions as in equation (4) and (5).

$$V^{+} = \{v_1, \ldots, v_n\} \quad \text{Positive ideal solution}$$

$$V^{-} = \{v_1', \ldots, v_n'\} \quad \text{Negative ideal solution}$$

Material	**Tensile Strength (MPa)**	**Young Modulus (MPa)**	**Flexural Stress (MPa)**	**Modulus of Elasticity (MPa)**	**Cost (RM)**
PLA/Wood 1	0.1085	0.0367	0.1385	0.1559	0.0591
PLA/Wood 2	0.1061	0.1178	0.0790	0.0684	0.0648
PLA/Coconut	0.0890	0.1148	0.0836	0.0846	0.1255
PLA/Bamboo	0.0951	0.1076	0.0872	0.0620	0.1287
V+ (best)	0.1085	0.1178	0.1385	0.1559	0.0591
V- (worst)	0.0890	0.0367	0.0790	0.0620	0.1287

IV. Next, step 4 involves in calculating the separation measures each alternative as in equation (6) and (7).

$$Si^{+} = [\sum (v_i - v_{ij})^2]^{1/2} \qquad i = 1,\ldots,m$$

Similarly, the separation from the negative ideal alternative is:

$$Si^{-} = [\sum (v_i - v_{ij})^2]^{1/2} \qquad i = 1,\ldots,m$$

V. Lastly, the data is calculated by the relative closeness to the ideal solution as in equation (8).

$$C_i = S'_i / (S_i + S'_i) \ , \ 0 < C_i < 1$$

Alternative which closes to 1 is selected.

Table 4-10 Result of TOPSIS method for material selection

Material	Si^+	Si^-	Performance Score		Rank
			$(Si^+)+(Si^-)$	C_i	
PLA/Wood 1	0.0811	0.1326	0.2137	0.6205	1
PLA/Wood 2	0.1060	0.1049	0.2109	0.4973	2
PLA/Coconut	0.1136	0.0815	0.1951	0.4178	3
PLA/Bamboo	0.1288	0.0716	0.2004	0.3575	4

According to the data in Table 4.9, the material with the greatest Ci value is PLA/Wood 1, which has a Ci of 0.6205. Conversely, PLA/Bamboo is positioned at the lowest end regarding this criterion, with a value of Ci 0.3575. Consequently, the evaluation favors the selection of PLA/Wood 1 as the optimal material for the fabrication procedure intended for the construction of the shark fin antenna. This conclusion arises from the exceptional performance exhibited by PLA/Wood 1 relative to the other materials assessed in this evaluation.

4.3 Discussion

4.3.1 Fabrication of Shark Fin Antenna

The process begins with the creation of a detailed three-dimensional model of the shark fin antenna using SolidWorks, a computer-aided design (CAD) software. This stage involves defining the geometry, dimensions, and surface features to ensure the design meets the intended specifications and functional requirements. SolidWorks provides robust tools for both surface and solid modeling, enabling precise control over the shape and structure of the antenna.

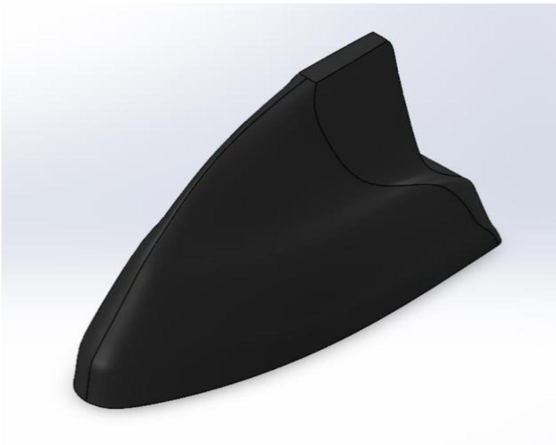

Figure 4-10 The Model Part

Once the design is finalized, the model must be exported in a format compatible with 3D printing software. The most common file format for this purpose is STL (stereolithography), which translates the model's surfaces into a mesh of triangles that can be interpreted by slicing software and 3D printers. The STL file preserves the geometric fidelity of the SolidWorks model and is widely accepted across various 3D printing platforms.

The exported STL file is then imported into slicing software, such as Bambu Studio. Slicing software prepares the model for 3D printing by converting the geometry into a series of horizontal layers and generating the corresponding toolpaths. During this phase, key parameters such as layer height, infill density, print orientation, support structures, and print speed are configured to optimize print quality and material usage. The slicing process results in a G-code file, which contains the step-by-step instructions for the 3D printer to follow. The generated G-code file is transferred to the 3D printer, commonly via SD card or direct USB connection. This file acts as the intermediary between the digital model and the physical manufacturing process, guiding the printer's movements and operations with high precision.

With the G-code loaded, the 3D printer such as the Bambu Lab P1P initiates the fabrication process. The printer deposits material layer by layer, following the instructions encoded in the G-code, to gradually build up the shark fin antenna. Throughout the process, the printer executes detailed movements to ensure dimensional accuracy and surface quality. The build may include supports or rafts to stabilize overhanging features and enhance bed adhesion, as specified during slicing. The printing parameters are as follows:

Table 4-11 Printing parameters for Fabrication

Parameter	Value
Nozzle temperature (°C)	220
Bed temperature (°C)	70
Percent infill (%)	100
Printing speed (mm/s)	100
Infill Pattern	Rectilinear
Layer height (mm)	0.2
Nozzle size (mm)	0.4
Adhesive	Blue tape and brim
Material type	PLA/wood
Support	Tree type

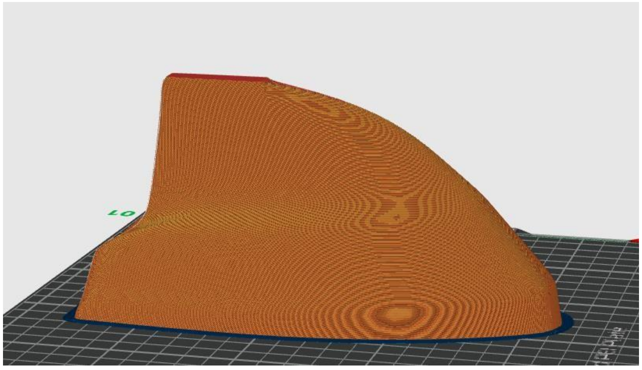

Figure 4-11 The Sliced Model

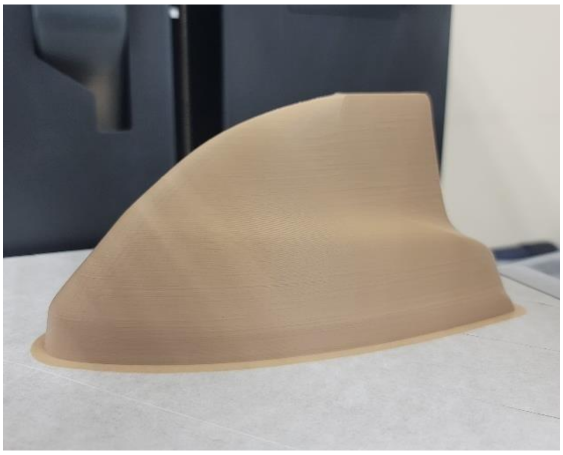

Figure 4-12 Printed Shark Fin Antenna

After printing is complete, the part is removed from the build platform. Any support structures or rafts are carefully detached, and the surface may undergo additional finishing processes such as sanding, polishing, or painting to achieve the desired appearance and functional characteristics.

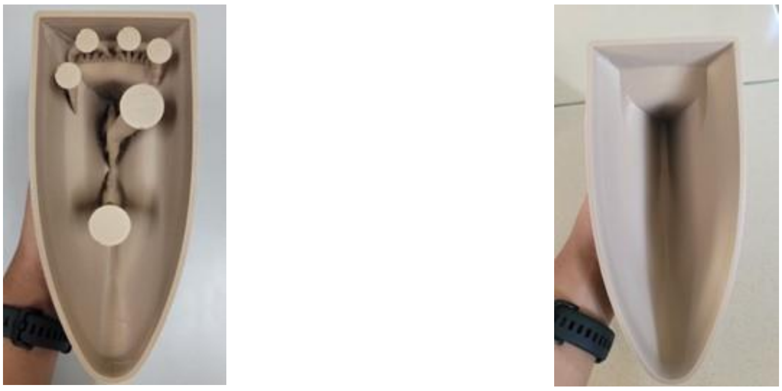

(a) (b)

Figure 4-13 The printed part

(a) before removing supports (b) after removing supports

The next step is to get the antenna ready to be put on the roof of the car once it meets the quality standards. It starts with a careful check of the antenna to make sure that the dimensions and surface quality are correct so that it fits perfectly on the mounting place. At the same time, any necessary mounting hardware, like brackets, gaskets, or adhesive pads, is made ready. Depending on the design, the antenna may also have built-in connectors or need wire harnesses to send signals. Before installation, the surface of the car roof is carefully cleaned to get rid of dust, oils, and other pollutants. This helps the adhesive stick better and keeps the roof from rusting. Finally, the shark fin antenna is carefully lined up and placed on the roof, usually above the antenna base or mounting point, where it will be securely attached.

Figure 4-14 Installed shark fin antenna
(a) front side (b) right side

4.3.2 Printing Issue and Solution

During the 3D printing process, a recurring issue encountered was warping, particularly when no adhesive measures such as a brim or blue tape, were applied to the print bed. As shown in Figure 4.15 (a), prints attempted without any additional adhesion aids consistently failed, with the base of the part lifting and deforming (warping) during the process.

Warping occurs when the extruded filament cools too rapidly or unevenly, causing the material to contract and pull away from the build plate. This results in the corners or edges of the print lifting, leading to dimensional inaccuracies or complete print failure. The lack of a brim and blue tape meant that the initial layers did not adhere sufficiently to the bed, making the print highly susceptible to this defect.

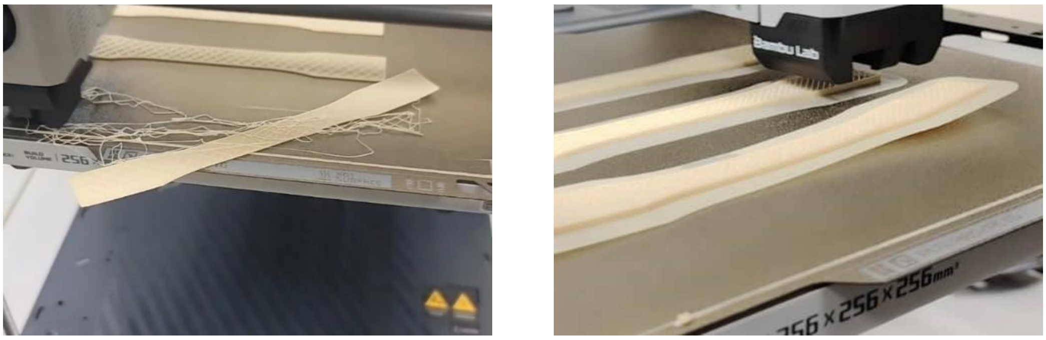

(a) (b)

Figure 4-15 The applied adhesive
(a) without brim and blue tape (b) brim applied

A 5 mm brim was added around the base of the print using slicing software. The brim increases the surface area in contact with the bed, significantly enhancing the adhesion of the first layers and anchoring the part during printing. Blue painter’s tape was applied to the print bed surface. The porous texture of blue tape provides additional grip for the extruded filament, further reducing the likelihood of warping, especially for materials prone to poor bed adhesion.

Figure 4-16 Brim and Blue tape applied

As depicted in Figure 4.16, the combined use of a brim and blue tape resulted in perfect prints, with no observable warping or lifting at the part's edges. The first layers adhered uniformly, allowing the print to proceed to completion without deformation.

CHAPTER 5
CLOSING

5.1 Conclusions

Based on the research that has been conducted, it is obtained some conclusions have been obtained, as follows: :

- A shark fin antenna was successfully developed using natural fiber composite (PLA/Wood) filaments and Fused Deposition Modeling (FDM) 3D printing, with three unique designs created and evaluated through SolidWorks Flow Simulation.
- Design 3 was identified as the most aerodynamic using the TOPSIS method, achieving a drag force of 0.457 N, coefficient of drag of 0.215, surface pressure of 101821.69 Pa, and a closeness coefficient (C_i) of 0.995.
- Mechanical testing (tensile and flexural) of PLA/Wood specimens showed that 100% infill density provided the best mechanical strength, proving that infill parameters significantly affect performance.
- PLA/Wood was confirmed as the optimal material, with a tensile strength of 37.46 MPa, Young's modulus of 1663 MPa, flexural stress of 65.187 MPa, modulus of elasticity of 2694 MPa, and a TOPSIS C_i value of 0.620.
- The study effectively combined simulation, experimental testing, and multi-criteria decision-making (TOPSIS) to achieve a well-balanced, sustainable, and high-performance design for 3D-printed shark fin antennas.

5.2 Suggestions

According to the research, there is knowledge learned along the way of this study. Lessons learned by this study can be reflected and implemented in the upcoming study, which are:

- Conduct real-world trials of the shark fin antenna to evaluate its aerodynamic performance and durability under actual environmental conditions such as weather changes, wind loads, and mechanical stress.
- Expand the number of design variations beyond the initial three models to explore alternative shapes, structural reinforcements, or hybrid configurations that could improve aerodynamic efficiency and mechanical performance.
- Integrate real-world testing with advanced simulation tools to validate and enhance the accuracy of laboratory and simulation results.

REFERENCE

AbouelNour, Y., Rakauskas, N., Naquila, G., Melnyk, A., & Ragai, I. (2024). Tensile testing data of additive manufactured ASTM D638 standard specimens with embedded internal geometrical features. *Scientific Data, 11*, 506.

Al Mohamed, A. A., Al Mohamed, S., & Zino, M. (2023). Application of fuzzy multicriteria decision-making model in selecting pandemic hospital site. *Future Business Journal, 9*(1), 14.

Alshahrani, H., & Ahmed, A. (2022). Study on flexural behavior of glass fiber reinforced plastic sandwich composites using liquid thermoplastic resin. *Polymers, 14*(19), 4045.

Ashby, M. F. (2016). *Materials Selection in Mechanical Design*. Netherlands: Butterworth-Heinemann.

ASTM International. (2015). *Standard test methods for flexural properties of unreinforced and reinforced plastics and electrical insulating materials (ASTM D790–15)*. Retrieved June 20, 2025, from https://www.zwickroell.com/industries/plastics/thermoplastics-and-thermosetting-molding-materials/tensile-properties-astm-d638/

Azman, M. A., Asyraf, M. R. M., Khalina, A., Petrů, M., Ruzaidi, C. M., Sapuan, S. M., Wan Nik, W. B., Ishak, M. R., Ilyas, R. A., & Suriani, M. J. (2021). Natural Fiber Reinforced Composite Material for Product Design: A Short Review. *Polymers*, *13*(12), 1917.

Bhayana, M., Singh, J., Sharma, A., & Gupta, M. (2023). *A review on optimized FDM 3D printed wood/PLA biocomposite material characteristics*. *Materials Today: Proceedings*.

Bi, X., & Huang, R. (2022). 3D printing of natural fiber and composites: A state-of-the-art review. *Materials & Design, 222*, 111065.

Cano-Vicent, A., Tambuwala, M. M., Hassan, S. S., Barh, D., Aljabali, A. A. A., Birkett, M., Arjunan, A., & Serrano-Aroca, Á. (2021). Fused deposition modelling: Current status, methodology, applications and future prospects. *Additive Manufacturing, 47*, 102378.

Cojocaru, V., & Miclosina, C.-O. (2020). Influence of rectilinear infill parameters on stress state of mechanical structures components. *Robotica & Management, 25*(2), 4–11.

Elseify, L., Midani, M., El-Badawy, A., & Jawaid, M. (2021). *Manufacturing automotive components from sustainable natural fiber composites*. In M. Jawaid, M. Thariq, & N. Saba (Eds.), Design and manufacture of sustainable automotive composites. Springer.

Erdebilli, B., Gecer, E., Yılmaz, İ., Aksoy, T., Hacıoğlu, U., Dinçer, H., & Yüksel, S. (2023). Q-ROF fuzzy TOPSIS and VIKOR methods for the selection of sustainable private health insurance policies. *Sustainability, 15*(12), 9229.

Erhunmwun, I. D., & Ikponmwosa, U. B. (2017). Review on finite element method. *Journal of Applied Sciences and Environmental Management, 21*(5), 999–1002.

Faidallah, R. F., Hanon, M. M., Vashist, V., Habib, A., Szakál, Z., & Oldal, I. (2023). Effect of Different Standard Geometry Shapes on the Tensile Properties of 3D-Printed Polymer. *Polymers*, *15*(14), 3029.

Fauzi, A. F. M. F., Wahid, Z., Mohd Radzuan, N. A., Abd Aziz, N., Juri, A. Z., & Sulong, A. B. (2024). *A study on mechanical performance of 3D printed wood mimic materials. Jurnal Kejuruteraan, 36*(6), 2571–2577.

Fountas, N. A., Papantoniou, I., Kechagias, J. D., Manolakos, D. E., & Vaxevanidis, N. M. (2021). Experimental investigation on flexural properties of FDM-processed PET-G specimens using response surface methodology. *MATEC Web of Conferences, 349*, 01008.

García-Domínguez, A., Claver, J., Camacho, A. M., & Sebastián, M. A. (2019). Considerations on the applicability of test methods for mechanical characterization of materials manufactured by FDM. *Materials, 13*(1), 28.

Güçlü, P. (2024). Comparative analysis of the MCDM methods with multiple normalization techniques: Three hybrid models combine MPSI with DNMARCOS, AROMAN, and MACONT methods. *Business and Economics Research Journal, 15*(2), 129–154.

Haider, N. A., & Jamal, K. (2024). Implementation of low-profile multiband planar antenna for Internet of Vehicle communication. *Wireless Personal Communications, 138*, 229–243.

Harpool, T. D., Alarifi, I. M., Alshammari, B. A., Aabid, A., Baig, M., Malik, R. A., Mohamed Sayed, A., Asmatulu, R., & El-Bagory, T. M. A. A. (2021). Evaluation of the infill design on the tensile response of 3D printed polylactic acid polymer. *Materials, 14*(9), 2195.

Hu, Z., Yang, R., Fang, L., Wang, Z., & Zhao, Y. (2024). Research on vehicle speed prediction model based on traffic flow information fusion. *Energy, 292*, 130416.

Jatti, V. S., Tamboli, S., Shaikh, S., Solke, N. S., Gulia, V., Jatti, V. S., Khedkar, N. K., Salunkhe, S., Pagáč, M., & Abouel Nasr, E. S. (2024). *Optimization of tensile strength in 3D printed PLA parts via meta-heuristic approaches: A comparative study. Frontiers in Materials, 10*, 1336837.

Jumaidin, R., Sapuan, S. M., Jawaid, M., Ishak, M. R., & Sahari, J. (2021). A review on natural fibers for development of eco-friendly bio-composites: Characteristics, processing and applications. *Materials Today: Proceedings, 42*, 2555–2560. https://doi.org/10.1016/j.matpr.2020.12.410

Kang, C. H., Kim, D. Y., Lee, C. H., Kim, K. H., & Choi, J. H. (2022). Design of a 5G Sub-6 GHz vehicular cellular antenna element with consistent radiation pattern using characteristic mode analysis. *Sensors, 22*(22), 8862.

Khilji, I. A., Chilakamarry, C. R., Surendran, A. N., Kate, K., & Satyavolu, J. (2023). Natural Fiber Composite Filaments for Additive Manufacturing: A Comprehensive Review. Sustainability, 15(23), 16171.

Khouri, N. G., Bahú, J. O., Blanco-Llamero, C., Severino, P., Concha, V. O. C., & Souto, E. B. (2024). *Polylactic acid (PLA): Properties, synthesis, and biomedical applications – A review of the literature*. *Journal of Molecular Structure, 1309*, 138243.

Koltsaki, M., & Mavri, M. (2024). A comprehensive overview of additive manufacturing processes through a time-based classification model. *3D Printing and Additive Manufacturing, 11*(1), 363–382.

Kulkarni, A. G., Satyanarayana, K. G., Rohatgi, P. K., & Vijayan, K. (2021). A comprehensive review on natural fibers: Technological and socio-economical aspects. *Materials Today: Proceedings, 46*, 5923–5928.

Kumar, A., & Singh, R. (2023). An integrated shark-fin reconfigurable antenna for V2X communications. *Academia.edu*. Retrieved April 23, 2025, from https://www.academia.edu/116763530/An_Integrated_Shark_Fin_Reconfigurable_Antenna_for_V2X_Communications

Medibew, M., & Tesfaye, T. (2022). A comprehensive review on the optimization of the fused deposition modeling process parameter for better tensile strength of PLA-printed parts. *Advances in Materials Science and Engineering*, 2022, Article 5490831, 11 pages.

Pavić, Z., & Novoselac, V. (2013, June). *Notes on TOPSIS method*. *International Journal of Research in Engineering and Science (IJRES), 1*(2), 5–12.

Ranakoti, L., Gangil, B., Mishra, S. K., Singh, T., Sharma, S., Ilyas, R., & El-Khatib, S. (2022). *Critical review on polylactic acid: Properties, structure, processing, biocomposites, and nanocomposites*. *Materials, 15*(12), 4312.

Rasiya, G., Shukla, A., & Saran, K. (2021). Additive manufacturing—A review. *Materials Today: Proceedings, 47*(Part 19), 6896–6901.

Sahib Dua, H., Khatri, H., Naveen, J., Jawaid, M., Jayakrishna, K., Norrrahim, M. N. F., & Rashedi, A. (2023). Potential of natural fiber based polymeric composites for cleaner automotive component production: A comprehensive review. *Journal of Materials Research and Technology*, *25*, 1086–1104.

Sahoo, D., Parida, P. K., & Pati, B. (2024). Efficient fuzzy multi-criteria decision-making for optimal college location selection: A comparative study of min–max fuzzy TOPSIS approach. *Results in Control and Optimization, 15*, 100422.

Sahoo, S. K., & Goswami, S. S. (2023). A comprehensive review of multiple criteria decision-making (MCDM) methods: Advancements, applications, and future directions. *Decision Making Advances, 1*(1), 25–48.

Sahoo, S. K., & Goswami, S. S. (2023). A comprehensive review of multiple criteria decision-making (MCDM) methods: Advancements, applications, and future directions. *Decision Making Advances, 1*(1), 25–48.

Saleh, S. A., Ibrahim, R. W., & Ahmed, S. A. (2020). A novel automobile antenna for vehicles communication of IoT systems in 5G network. *EURASIP Journal on Wireless Communications and Networking, 2020*(1), 218.

Sanchez-Lozano, J., Larraz, M. A., & Fernandez-Martinez, M. (2022). *A comparison between fuzzy TOPSIS and VIKOR to the selection of aircraft for airspace defense*. SSRN.

Satsum, A., Busayaporn, W., Rungswang, W., & others. (2022). *Structural and mechanical properties of biodegradable poly(lactic acid) and pectin composites: Using bionucleating agent to improve crystallization behavior*. *Polymer Journal, 54*, 921–930.

Saurabh, & Yadav, Y. (2016). Literature review on finite element method. *International Journal of Enhanced Research in Science, Technology & Engineering, 5*(3), 267–269.

Servaitė, D., Užupytė, R., & Krilavičiusa, T. (2020). *Logistics service provider selection using TOPSIS and VIKOR methods*. In *CEUR Workshop Proceedings* (Vol. 2698, p. 13). CEUR-WS.org.

Setiawan, A., Arumi, E. R., & Sukmasetya, P. (2020). Fuzzy membership functions analysis for usability evaluation of online credit hour form. *Journal of Engineering Science and Technology, 15*(5), 3189–3203.

Shadrach, L. S., Daniel, M. S., & Samuel, J. (2021). A review on development of natural fibre composites for industrial applications. *Journal of Materials Science and Chemical Engineering, 9*(3), 23–38.

Shaharuzaman, M. A., Jumaidin, R., Mohd Adrinata, S. M., Idros, S. M. A. S., Mansor, M. R., & Senan, H. (2024). Conceptual design and materials selection of the FDM composites for passenger vehicle's spoiler. *Pertanika Journal of Science & Technology, 32*(S2), Article 01008.

Singh, S., Muthusamy, K., & Nuruddin, M. F. (2023). Advantages of natural fiber composites for biomedical applications. *Innovative Infrastructure Solutions, 8*(4), 1–8.

Taherdoost, H., & Madanchian, M. (2023). VIKOR method—An effective compromising ranking technique for decision making. *Macro Management & Public Policies, 5*(2), 27–33.

Triawan, F., Syefira, D., Rismalia, M., Suryani, I. O., Djamari, D. W., Budiman, B. A., Arief Budiman, B., & … Nandianto, A. B. D. (2022). The influence of infill density and pattern on the mechanical and fracture behavior of 3D printed structure subjected to uniaxial tensile load. *Journal of Engineering Science and Technology, 17*(5), 3254–3266.

Vafaei, N., Ribeiro, R. A., & Camarinha-Matos, L. M. (2018). Data normalisation techniques in decision making: Case study with TOPSIS method. *International Journal of Information and Decision Sciences, 10*(1), 19–38.

Vassoney, E., Mammoliti Mochet, A., Desiderio, E., Negro, G., Pilloni, M. G., & Comoglio, C. (2021). Comparing multi-criteria decision-making methods for the assessment of flow release scenarios from small hydropower plants in the Alpine area. *Frontiers in Environmental Science, 9*, 635100.

Vyavahare, S., & Teraiya, S. (2020). Fused deposition modelling: A review. *Rapid Prototyping Journal, 26*(1), 176–201.

Wu, Y., Lu, Y., Zhao, M., Bosiakov, S., & Li, L. (2022). A critical review of additive manufacturing techniques and associated biomaterials used in bone tissue engineering. *Polymers, 14*(10), 2117.

Xu, X., Zhang, Y., Xu, Z., Liao, H., & Tong, Z. (2024). Multi-attribute decision making based on VIKOR with probabilistic linguistic term sets: An application to the risk evaluation of foreign direct investment. *PLOS ONE, 19*(3), e0294758.

Zakeri, S., Chatterjee, P., Konstantas, D., Loni, H. A., Rezaei, N., & Ghadimi, N. (2023). A decision analysis model for material selection using simple ranking process. *Scientific Reports, 13*, 8631.

Zhai, X., Jin, L., & Jiang, J. (2022). A survey of additive manufacturing reviews. *Materials Science in Additive Manufacturing, 1*(4), 21.

Zhang, Y., Wei, F., Zhang, Z., & Li, D. (2024). Combined shark-fin rooftop antenna for LTE, WLAN and BeiDou applications. *Electronics, 13*(7), 1324.

Zulkifli, I. S. M., Singh, S. S. S., Shankar, K. A., Wong, F. R., & Nor Ma'arof, M. I. (2020). Tensile test of fly-ash-HDPE hybrid composite via finite element analysis. *INTI Journal, 2020*(27).

Zulkifli, R., Ahmad, Z., Mohd Rafie, A. S., & Majid, M. S. A. (2023). A comprehensive review of natural fibers and their composites. *Emerging Materials Research, 12*(2), 151–166.

ZwickRoell. (n.d.). *ASTM D638 tensile properties of plastics*. ZwickRoell. Retrieved June 20, 2025, from https://www.zwickroell.com/industries/plastics/thermoplastics-and-thermosetting-molding-materials/tensile-properties-astm-d638/

APPENDIX 1

DRAWING SHARK FIN ANTENNA

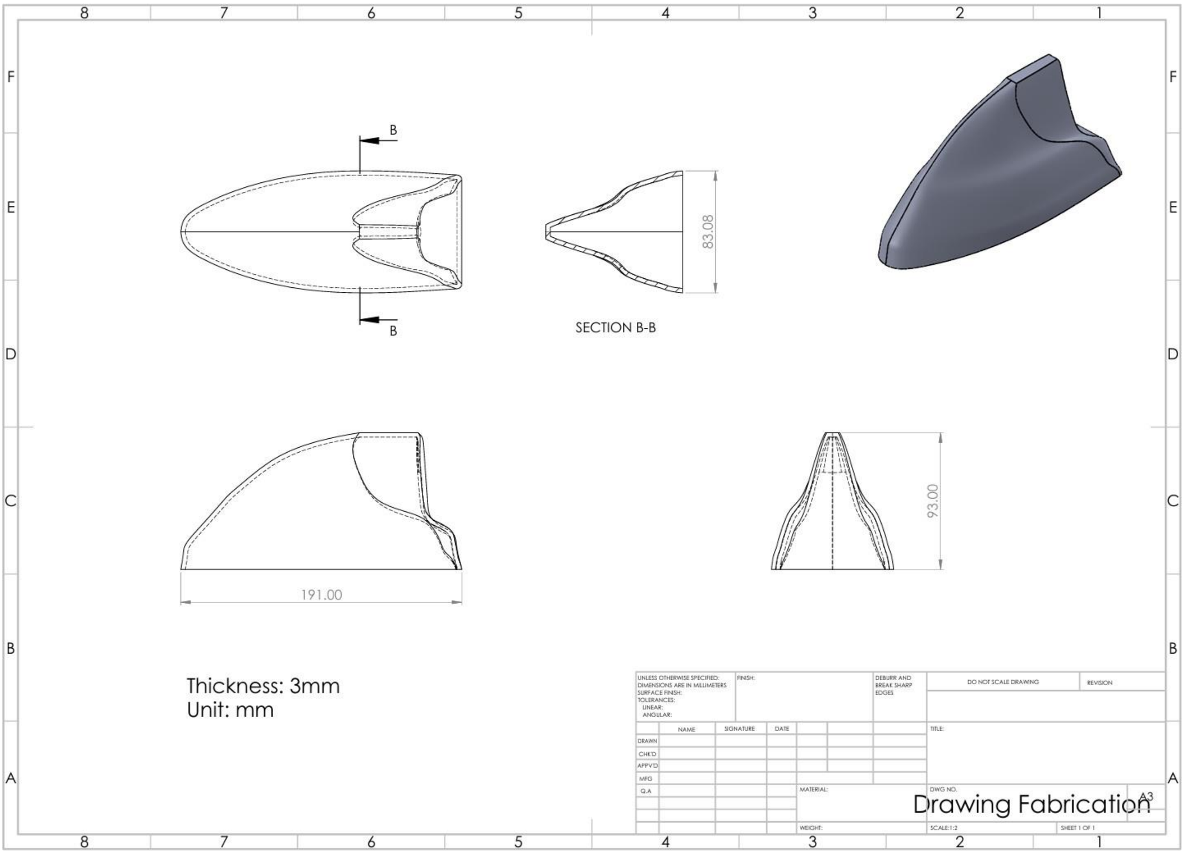

UNIVERSITI TEKNIKAL MALAYSIA MELAKA
FAKULTI TEKNOLOGI DAN KEJUTERAAN MEKANIKAL

BORANG PENGESAHAN STATUS LAPORAN

Tajuk Projek : Materials and Design Selection of NFC filament for the Shark Fin Antenna using Hybrid Method

Sesi Pengajian :

Saya Muhammad Mizan Abhiyasa mengaku membenarkan laporan Projek Sarjana Muda ini disimpan di Perpustakaan Laman Hikmah dengan syarat-syarat kegunaan seperti berikut:

1. Laporan adalah hakmilik Universiti Teknikal Malaysia Melaka.
2. Perpustakaan dibenarkan membuat salinan untuk tujuan pengajian sahaja.
3. Perpustakaan dibenarkan membuat salinan laporan ini sebagai bahan pertukaran antara institusi pengajian tinggi.
4. Sila tandakan (✓):

☐	**SULIT***	(Mengandungi maklumat yang berdarjah keselamatan atau kepentingan Malaysia sepertiyang termaktub di dalam AKTA RAHSIA RASMI 1972).
☐	**TERHAD***	(Mengandungi maklumat terhad yang telah ditentukan oleh organisasi/badan di mana penyelidikan dijalankan)
✓	**TIDAK TERHAD**	

Disahkan oleh:

Muhammad Mizan Abhiyasa
(TANDATANGAN PENULIS)

Ts. Dr Mohd Adrinata bin Shaharuzaman
(COP DAN TANDATANGAN PENYELIA)

MOHD ADRINATA BIN SHAHARUZAMAN
PENSYARAH KANAN
FAKULTI KEJURUTERAAN MEKANIKAL
UNIVERSITI TEKNIKAL MALAYSIA MELAKA

Alamat Tetap:

Tarikh:

Tarikh: 15 July 2025